Mon. Not. R. Astron. Soc. **371,** 263–282 (2006) doi:10.1111/j.1365-2966.2006.10641.x

The mass of helium in white dwarf stars and the formation and evolution of hydrogen-deficient post-AGB stars

T. M. Lawlor[1⋆] and J. MacDonald[2⋆]

[1] *Penn State University – Wilkes-Barre Campus, Department of Physics, Lehman, PA 18627, USA*
[2] *University of Delaware, Department of Physics and Astronomy, Newark, DE 19716, USA*

Accepted 2006 May 31. Received 2006 May 30; in original form 2006 February 8

ABSTRACT

We use two sets of 'cradle-to-grave' evolutionary calculations to investigate how the mass of the helium buffer layer between the CO core and the hydrogen-burning shell in thermally pulsing asymptotic giant branch (AGB) stars depends on the initial stellar mass and heavy element abundance. Cool star mass loss is included by augmenting the Reimers' formula with fits to mass-loss rates observed for Galactic Mira variables, obscured Large Magellanic Cloud (LMC) AGB variables and Galactic OH/IR sources. Resulting white dwarf masses are in good agreement with the semi-empirical final mass–initial mass relation. We derive lower and upper limits on the mass of helium in white dwarfs as functions of their mass and initial heavy element abundance. We find that stars that experience a very late thermal pulse (VLTP) have final helium masses that are about 25 per cent below the lower limit for stars that do not experience a VLTP. We have derived a modified form of Iben's criterion for a star to experience a post-AGB helium shell flash, and subcriteria for discriminating between the occurrence of late and VLTPs. We find that a post-AGB flash does not necessarily result in formation of a non-DA white dwarf. Furthermore, we find that the relative amount of time spent burning helium or hydrogen depends on how the mass-loss rate varies with stellar surface parameters. These two considerations complicate the relationship between the probability that a star experiences a post-AGB flash and the relative formation rates of DA and non-DA white dwarfs. However, our calculations do lead to a non-DA/DA ratio that is consistent with the observed ratio.

We find that our predicted abundances for PG1159 stars agree within the error bars with the observed abundances, without the need of convective overshoot. We also find that nitrogen is produced during VLTPs but not in the other evolutionary paths to hydrogen-deficient objects. Hence, we propose this as the reason why nitrogen is observed in some PG1159 stars but not all. Our VLTP models also produce surface abundances close to those of the low-gravity hybrid PG1159 stars.

An inconsistency between asteroseismological and our evolutionary model determinations of helium layer mass remains.

Key words: stars: AGB and post-AGB – stars: evolution – white dwarfs.

1 INTRODUCTION

The mass, $M_{\rm buf}$, of the helium buffer layer which lies between the CO core and the hydrogen-burning shell in thermally pulsing asymptotic giant branch (AGB) stars is an important parameter for a number of reasons (Iben 1987). When the star leaves the AGB, $M_{\rm buf}$ not only determines whether a post-AGB helium flash will occur but also determines whether such a flash occurs as a late thermal pulse (LTP) during the planetary nebula phase or as a very late thermal pulse (VLTP) after the star has entered the white dwarf cooling phase. These LTPs and VLTPs have direct bearing on the formation of non-DA white dwarfs (Renzini 1979; Schönberner 1979; Iben et al. 1983; Iben 1984; Wood & Faulkner 1986; Vassiliadis & Wood 1994; Iben, Tutukov & Yungelson 1996; Herwig et al. 1999; Blöcker 2001) and hydrogen-deficient planetary nebulae, such as Abell 30 and Abell 78 (Renzini 1983; Iben 1984; Iben et al. 1996), and have been proposed as the cause of the born-again (hereafter BA) phenomenon exhibited by FG Sge, V4334 Sgr (= Sakurai's object) and V605 Aql (Iben & MacDonald 1995; Blöcker & Schönberner 1997; Herwig 2001; Lawlor & MacDonald 2003). The final value of $M_{\rm buf}$ controls the amount of C and O that can be convectively

⋆E-mail: tlawlor@psu.edu (TML); jimmacd@udel.edu (JM)

dredged to the surface in DQ white dwarfs (Koester, Weidemann & Zeidler 1982; Pelletier et al. 1986; MacDonald, Hernanz & Jose 1998). It also determines whether a white dwarf can experience a final hydrogen shell flash due to inward diffusion of hydrogen and outward diffusion of carbon into regions hot enough for nuclear reactions to occur (Iben & MacDonald 1986). Also, asteroseismological studies of DBv white dwarfs have been used to probe their interior structure and to place constraints on $M_{\rm buf}$ (Bradley & Winget 1994; Fontaine & Brassard 2002; Metcalfe, Montgomery & Kawaler 2003).

In this paper, we use two sets of 'cradle-to-grave' evolutionary calculations to investigate how $M_{\rm buf}$ depends on the initial stellar mass and heavy element abundance. In Section 2, we give a brief description of the stellar models and the stellar evolution program. In Section 3, we compare the evolutionary stages prior to the thermal pulsing AGB phase with earlier studies, and in Section 4 we describe the properties of the thermal pulses. In Section 5, we use the semi-empirical initial mass–final mass relation to justify our treatment of mass loss and our neglect of convective overshoot. In Section 6, we give details of the final white dwarf hydrogen and helium layer masses. In Section 7, we revisit the Iben (1987) criterion for the occurrence of post-AGB helium shell flashes. Discussion and conclusions are given in Sections 8 and 9.

2 THE STELLAR MODELS AND THE STELLAR EVOLUTION PROGRAM

2.1 The stellar models

In the first set of calculations, 1.0 $M_\odot$ stars with heavy element abundances $Z = 10^{-3}, 4 \times 10^{-3}, 10^{-2}$ and 2×10^{-2} have been evolved from the pre-main sequence (PMS) to white dwarf cooling track. Mass loss was taken into account by using a scaled Reimers' mass-loss law (Reimers 1975). To mimic the effects of small differences in mass-loss rate, we varied the mass-loss rate starting from the peak of the last AGB thermal pulse by choosing different values for the Reimers' mass-loss parameter, η. This gives a complete range of the possible helium layer masses at the point when the star leaves the AGB for the first time. These calculations have been used by Lawlor & MacDonald (2003; hereafter LM03) to argue that the BA stars V4334 Sgr, V605 Aql and FG Sge lie at different points along a common evolutionary path, and hence we will refer to this set of models as the LM03 set. In the second set of calculations, stars of masses in the range 0.1–100 $M_\odot$ and $Z = 2 \times 10^{-4}$, 10^{-3}, $4 \times 10^{-3}, 10^{-2}, 2 \times 10^{-2}, 5 \times 10^{-2}$ and 10^{-1} have been evolved with mass loss from the PMS to an end point that depends on the initial stellar mass. The evolution of low-mass stars ($M \leqslant 3\,M_\odot$) is ended at the earlier of settling on to the white dwarf cooling sequence and reaching an age of 20 Gyr. The evolution of massive stars ($M \geqslant 10\,M_\odot$) is stopped at the earlier of the end of carbon burning or the central temperature exceeding 10^9 K. For the intermediate-mass stars, the calculation is stopped at the beginning of hydrodynamical ejection of the outer layers due to the radiative luminosity exceeding the local Eddington limit. In addition to the Reimers' mass loss (with a fixed value of η), we use a fit to observe mass-loss rates of Mira variables and OH/IR sources to account for mass loss during AGB evolution. This set of calculations has been used by Jimenez et al. (2004) to produce synthetic stellar population predictions of the integrated emission from star clusters and galaxies of arbitrary age, and hence we will refer to this set of models as the JM04 set.

For both sets of calculations, the helium mass fraction, Y, is related to the heavy element abundance by

$$Y = 0.235 + 2Z \tag{1}$$

except for $Z = 0.1$ for which we use $Y = 0.485$. The dependence in equation (1) is predicated on the assumption that nuclear processes in stars produce helium in linear proportion to heavy elements. Our values for the primordial helium abundance and dY/dZ are taken from Peimbert, Peimbert & Luridiana (2002) and Jimenez et al. (2003).

2.2 The stellar evolution program

Because the two sets of models have been calculated with slightly different versions of the stellar evolution code, we give a description of the code here. Our code is a much modified version of the Eggleton code (Eggleton 1971, 1972). The whole star is evolved by a relaxation method without the use of separate envelope calculations. Some of the advantages of this approach are that (i) gravothermal energy generation terms are automatically included for the stellar envelope, (ii) mass loss occurs at the stellar surface rather than an interior point of the star and (iii) the occurrence of convective dredge-up of elements produced by nucleosynthesis in the interior to the photosphere is clearly identifiable. For numerical stability reasons, a staggered mesh is used (Sugimoto 1970). Our code uses a time-dependent adaptive mesh technique similar to that of Winkler, Norman & Newman (1984) in which advection terms are approximated by using second-order upwind finite differences. Convective energy transport is modelled by using the version of mixing-length theory described by Mihalas (1970). Composition equations for H, ^{3}He, ^{4}He, ^{12}C, ^{14}N, ^{16}O and ^{24}Mg are solved simultaneously with the structure and adaptive mesh equations. For a few calculations, ^{13}C is also explicitly included, with neutrons produced by the ^{13}C (α, n) ^{16}O reaction assumed to be instantly absorbed by heavy elements. Composition changes due to convective mixing are modelled in the same way as Eggleton (1972) by adding diffusion terms to the composition equations. We use a diffusion coefficient, $\sigma_{\rm con}$, that is consistent with mixing-length theory (Eggleton 1972; Iben & MacDonald 1995; Jimenez *et al.* 1996),

$$\sigma_{\rm con} = \beta w_{\rm con} l, \tag{2}$$

where $w_{\rm con}$ is the convective velocity, l is the mixing length and β is a dimensionless convective mixing efficiency parameter, which for isotropic turbulence would be equal to 1/3. We have experimented with different values for β in the range 10^{-4}–1. We find that for most stages of stellar evolution, the results are insensitive to the particular value of β because mixing time-scales are usually much shorter than the evolution time-scales. However, smaller values of β lead to smoother evolution and hence we set $\beta = 10^{-4}$. To treat semiconvection in the same way as Eggleton (1972) with our staggered mesh, we found that the opacity that enters into evaluation of $\sigma_{\rm con}$ at the edges of convection zones has to be evaluated on the convective side of the boundary. Everywhere else a geometric average is used. This procedure leads to the difference of radiative and adiabatic gradients smoothly approaching zero as the edge of a convection zone is approached from the inside. Mixing due to convective overshooting is not included. OPAL radiative opacities (Iglesias & Rogers 1996) are used for temperatures (in K) above $\log_{10}T = 3.84$. For temperatures below $\log_{10}\,T = 3.78$, we use opacities kindly supplied by David Alexander that have been calculated by the method of Alexander & Ferguson (1994). Between these temperatures limits, we interpolate between the OPAL and Alexander opacities. Pair and photoneutrino

loss rates are from Beaudet, Petrosian & Salpeter (1967) with modifications for neutral currents (Ramadurai 1976). Plasma neutrino rates are from Haft, Raffelt & Weiss (1994) and bremsstrahlung neutrino losses rates are from Itoh & Kohyama (1983). The equation of state is determined by minimization of a model free energy (see e.g. Fontaine, Graboske & van Horn 1977) that includes contributions from internal states of the H_2 molecule and all the ionization states of H, He, C, N, O and Mg. Electron degeneracy is included by the method of Eggleton, Faulkner & Flannery (1973). Coulomb and quantum corrections to the equation of state follow the prescription of Iben, Fujimoto & MacDonald (1992), with the Coulomb free energy updated to use the results of Stringfellow, DeWitt & Slattery (1990). Pressure ionization is included in a thermodynamically consistent manner by use of a hard-sphere free-energy term (Mansoori et al. 1971).

One difference between the codes used for the two sets of models is that for the JM04 set nuclear reaction rates are from the NACRE compilation (Angulo et al. 1999), whereas for the LM03 set older reaction rates from Fowler, Caughlan & Zimmerman (1975), Harris et al. (1983), Nomoto, Thielemann & Miyaji (1985), Caughlan & Fowler (1988) and Arnett (1996) were used. Weak screening corrections from Salpeter & van Horn (1969) and strong screening corrections from Itoh et al. (1979) were used for both sets of calculations.

For both sets of models, we use a scaled Reimers' (1975) law

$$\dot{M} = -4 \times 10^{-13} \eta \frac{L}{\mathrm{L}_\odot} \frac{R}{\mathrm{R}_\odot} \left(\frac{M}{\mathrm{M}_\odot} \right)^{-1} \mathrm{M}_\odot \ \mathrm{yr}^{-1} \quad (3)$$

for mass loss by cool star winds ($T_{\rm eff} \leqslant 10^4$ K). The dimensionless parameter η was taken to be 0.35 for the LM03 set. A slightly different value $\eta = 0.378$ was used for the JM04 set. These particular values are consistent with the mean value of η needed to produce observed globular cluster horizontal branch (HB) morphologies (Jimenez *et al.* 1996). While the Reimers' formula is adequate for the purposes of the LM03 study of 1.0 $\mathrm{M}_\odot$ stars, it severely underestimates the mass-loss rate during the later 'superwind' phases of more massive AGB stars (Renzini 1981; Willson 2000). To allow for this increase in mass-loss rate, we add for the AGB phases of the JM04 calculations, empirical relationships between the mass-loss rates from Mira variables and OH/IR sources and their pulsation periods. A fit to the mass-loss rates from galactic Mira variables determined by Knapp et al. (1998) from CO line emission measurements gives in terms of the pulsation period in days, P,

$$\dot{M} = -10^{-22.8} P^{6.32} \ \mathrm{M}_\odot \ \mathrm{yr}^{-1} \quad (4)$$

for stars with $P \leqslant 700$ d. Longer period objects are in general OH/IR sources for which the CO emission lines do not give reliable determinations of mass-loss rate (Heske et al. 1990). Lepine, Ortiz & Epchtein (1995) find from near-infrared photometry that, after averaging over similar objects, the mass-loss rate of OH/IR sources increases with the stellar luminosity but the rate of increase is lower for the more luminous objects. Whitelock et al. (2003) find that obscured AGB variables in the Large Magellanic Cloud (LMC) follow an extrapolation of the period–luminosity relation determined for stars of shorter period. Hence, the mass-loss rate for the long period OH/IR sources is also expected to increase with the pulsation period but with a weaker dependence than for the shorter period variables. We show in Fig. 1, mass-loss rates against pulsation period for the Knapp et al. (1998) sample of Galactic Mira variables, the Whitelock et al. (2003) sample of obscured LMC AGB variables and the averaged mass-loss rates of the Lepine et al. sample of Galactic OH/IR sources assuming that these objects obey the period–luminosity relation for O-rich Miras (Feast et al. 1989; Whitelock et al. 1994) or C-rich Miras (Groenewegen & Whitelock 1996). Also shown is our fit to the Knapp et al. (1998) data. We see that for $P \leqslant 700$ d, the data for the LMC stars overlap the data for the galactic Miras, which indicates that the effects of heavy element abundance differences are smaller than the scatter in the data. At longer periods, the mass-loss rates are lower than would be given by extrapolation of our fit for the shorter period variables. Hence, for $P \geqslant 620$ d, we use

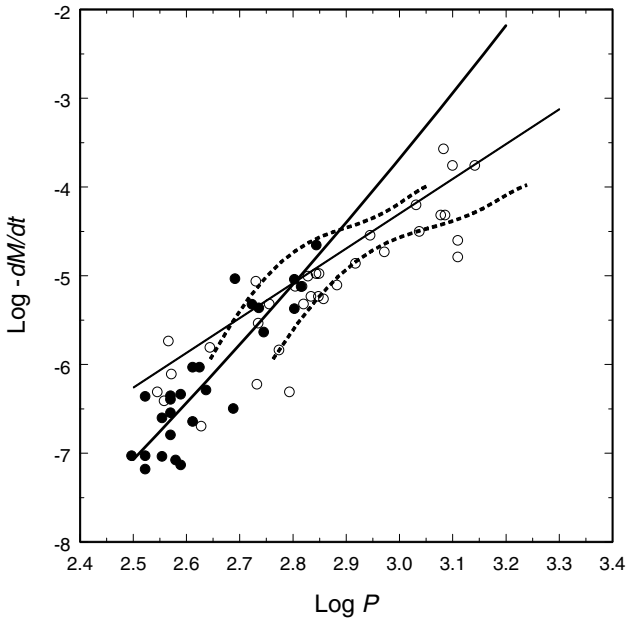

Figure 1. Mass-loss rate ($\mathrm{M}_\odot$ yr^{-1}) plotted against pulsation period (d) for Galactic Mira variables (filled circles), obscured LMC AGB variables (open circles) and Galactic OH/IR sources (broken lines). The thick and thin solid lines are the adopted relation for variables with periods less than 620 d and greater than 620 d, respectively.

$$\dot{M} = -10^{-16.1} P^{3.92} \ \mathrm{M}_\odot \ \mathrm{yr}^{-1}. \quad (5)$$

This relation is also shown in Fig. 1.

To relate the mass-loss rate to stellar surface properties, we assume that the AGB variables are pulsating in the fundamental mode with period (Ostlie & Cox 1986)

$$P = 1.2 \times 10^{-2} \left(\frac{M}{\mathrm{M}_\odot} \right)^{-0.73} \left(\frac{R}{\mathrm{R}_\odot} \right)^{1.86} \ \mathrm{d}. \quad (6)$$

For hot star winds ($T_{\rm eff} \geqslant 10^4$ K), we use a modified form of the theoretical mass-loss law of Abbott (1982) that has a heavy element abundance dependence that is closer to that of more recent theoretical calculations (Kudritzki, Pauldrach & Puls 1987; Kudritzki & Puls 2000; Vink, de Koter & Lamers 2001)

$$\dot{M} = -1.2 \ 10^{-15} \left(\frac{Z}{\mathrm{Z}_\odot} \right)^{1/2} \left(\frac{L}{\mathrm{L}_\odot} \right)^{2} \left(\frac{M_{\rm eff}}{\mathrm{M}_\odot} \right)^{-1} \mathrm{M}_\odot \ \mathrm{yr}^{-1}. \quad (7)$$

Here, $M_{\rm eff}$ is the mass of the star multiplied by a factor to account for the reduction of the effective gravity due to the radiative force on electrons. Because the Abbott (1982) mass-loss rate formula was originally developed for massive main-sequence (MS) stars, its use for the hot late stages of evolution of low-mass stars is open to question. We use it for these stages primarily because of its simplicity. However, as can be seen in Fig. 2, the formula gives mass-loss rates in fair agreement with those determined for central

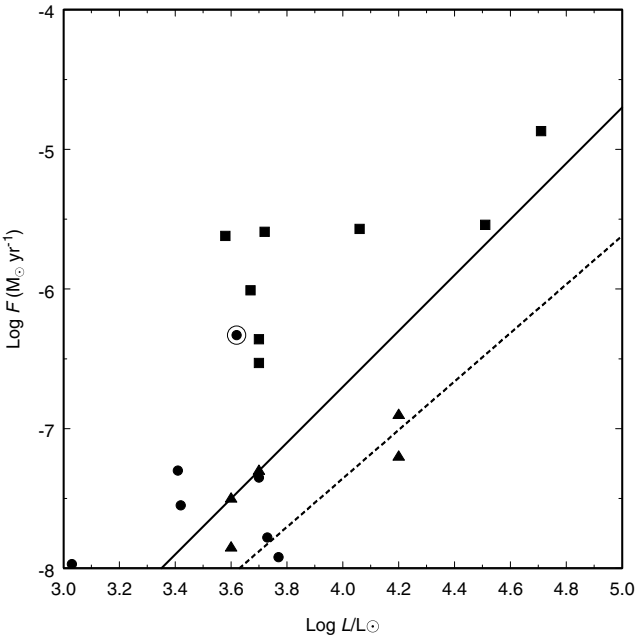

Figure 2. Mass-loss rate plotted against luminosity for PG1159 stars (filled triangles), CSPN in the LMC (filled circles) and WCL CSPN (filled squares). The open circle indicates a H-poor LMC CSPN. Also shown are the mass-loss rates from equation (7) for solar heavy element abundance and stellar mass 0.6 $M_\odot$ (solid line) and a fit to the Pauldrach et al. (1988) theoretical CSPN wind mass-loss rates (dashed line).

stars of planetary nebulae (CSPN) and PG1159 stars. In this figure, we plot against luminosity the mass-loss rate from equation (7) for solar heavy element abundance and stellar mass 0.6 $M_\odot$ together with empirical determinations of mass-loss rates for PG1159 stars (Koesterke & Werner 1998), CSPN in the LMC (Herald & Bianchi 2004) and CSPN of spectral-type WCL (Leuenhagen, Hamann & Jeffery 1996). Also shown is a fit to the Pauldrach et al. (1988) theoretical CSPN wind mass-loss rates for solar abundance material. Not surprisingly the empirical mass-loss rates for the WCL CSPN are higher than the theoretical rates, just as mass-loss rate determinations for Wolf–Rayet (WR) stars are higher than theoretical rates for MS OB stars. The mass-loss mechanism for WR stars is poorly understood but it is thought that helium enhancement is involved in producing higher mass-loss rates. However, this cannot be the whole story as the PG1159 stars have high helium abundances in their atmospheres, yet their mass-loss rates are close to the theoretical values. An added complication is that the LMC CSPN and WCL CSPN mass-loss rate determinations are based on spherically symmetric models, whereas filling factors due to clumping of 0.1 are typical for WR winds (Hillier 2003; Schild et al. 2004). Clumping reduces the empirical mass-loss rates in proportion to the square root of the filling factor, and hence the smooth mass-loss rates give only an upper limit to the true rates. Because of these uncertainties, a clear choice between the equation (7) mass-loss formula and the Pauldrach et al. (1988) mass-loss rates cannot be made. We will briefly return to this question in the discussion.

3 EVOLUTION TO THE THERMALLY PULSATING AGB

All of our JM04 evolutionary sequences begin on the PMS with a central temperature close to 10^6 K. They are evolved through all evolutionary phases, including the helium core flash that occurs in stars of mass less than about 2.5 $M_\odot$, to the end point described in Section 2.1. To allow for comparison with other calculations, we summarize lifetimes of the various evolutionary phases in Table 1. The PMS lifetime, $\tau_{\rm PMS}$, is the time to reach the minimum in luminosity at the start of MS evolution. The MS lifetime, $\tau_{\rm MS}$, is the time from the end of the PMS for the central hydrogen mass fraction to drop to zero. The time $\tau_{\rm CHeI}$ is the interval from the end of the MS to core helium ignition, which we take to occur when the rate of energy production by helium burning first becomes 10 per cent of the rate of energy production by hydrogen burning. This interval includes the subgiant phase and first red giant branch (RGB) phase. For those stars that experience a core helium flash, we give $\tau_{\rm CHeF}$, the time interval from helium ignition to the point at which star settles into a thermal equilibrium state, which we take to be when gravothermal energy production is less than 1 per cent of energy production from nuclear reactions. The core helium-burning lifetime to the point where the helium mass fraction at the stellar centre drops to 10^{-5} is $\tau_{\rm CHeB}$. For models that reach the thermal pulse phase before carbon ignition, we give the early AGB (EAGB) lifetime, $\tau_{\rm EAGB}$, which is the time from the end of core helium burning to the first major shell flash, and the thermally pulsing AGB lifetime, $\tau_{\rm TAGB}$, which is time between the peak of the first helium shell flash and departure from the AGB.

MS lifetimes increase with Z up to $Z = 0.02$. They decrease at higher Z because the smaller hydrogen mass fraction leads to a shorter time for core hydrogen exhaustion. MS stars with $M > \sim 1.2\ M_\odot$ have convective cores and hence $\tau_{\rm MS}$ will depend on the amount of mixing by convective overshooting that is included in the models. Since we do not include convective overshooting in our models, we expect that our models will have shorter MS lifetimes than models that include convective overshooting. Comparisons with the Geneva models (Schaller et al. 1992; Mowlavi et al. 1998; Lejeune & Schaerer 2001) and Padua models (Girardi et al. 2000) show that this indeed the case. For the Geneva models, our MS lifetimes agree within 2 or 3 per cent for stars which have radiative cores ($M < \sim 1.2\ M_\odot$). However, for stars with convective cores, the Geneva MS lifetimes are significantly longer than ours by about 35 per cent for $Z = 0.001$ and up to 50 per cent for $Z = 0.02$ and 0.1. On comparison with the Padua models for $Z = 0.001$ and 0.004, we find that our MS lifetimes are about 9 per cent longer for the stars with radiative cores and up to 30 per cent shorter for the more massive stars with convective cores.

Understanding the effects of convective overshooting on helium-burning lifetimes is less straightforward than for the MS lifetimes. Convective overshooting during MS evolution will produce larger helium cores. Hence, we might expect the model star to evolve at a faster rate similar to that of a more massive model star that does not include convective overshoot. However, convective overshoot during core helium burning will mix more helium into the core and this will increase $\tau_{\rm CHeB}$. It is these competing effects that make comparison difficult. A further complication is the existence of breathing pulses (Castellani, Giannone & Renzini 1971; Castellani et al. 1985), which can occur near the end of core helium burning. During a breathing pulse, the convective core expands and mixes fresh helium into the burning region which extends the core helium-burning phase. Hence, models which suppress breathing pulses will have smaller values for $\tau_{\rm CHeB}$. We do not suppress breathing pulses. Even so, for $M \lesssim 2.5\ M_\odot$, our values for $\tau_{\rm CHeB}$ are in general less than those found by Vassiliadis & Wood (1993) who do not include convective overshoot but do suppress breathing pulses. Our core helium-burning lifetimes are in general longer than the Geneva lifetimes, especially for the higher mass models. This is consistent

Table 1. Lifetimes of evolutionary phases.

$M/M_\odot$	Z	τ_{PMS} (yr)	τ_{MS} (yr)	τ_{CHeI} (yr)	τ_{CHeF} (yr)	τ_{CHeB} (yr)	τ_{EAGB} (yr)	τ_{TAGB} (yr)	τ_{AGB}/τ_{CHeB}
0.9	0.0002	2.50×10^7	8.61×10^9	9.98×10^8	2.39×10^6	9.01×10^7	1.09×10^7	1.45×10^6	0.137
1.0	0.0002	2.02×10^7	5.83×10^9	8.17×10^8	2.06×10^6	8.49×10^7	1.12×10^7	1.88×10^6	0.154
1.2	0.0002	1.46×10^7	3.00×10^9	5.53×10^8	1.61×10^6	8.73×10^7	1.02×10^7	2.21×10^6	0.142
1.5	0.0002	9.05×10^6	1.33×10^9	3.68×10^8	9.41×10^6	8.33×10^7	8.81×10^6	2.14×10^6	0.131
2.0	0.0002	4.44×10^6	5.42×10^8	1.44×10^8	3.03×10^6	1.05×10^8	5.67×10^6	1.81×10^6	0.071
3.0	0.0002	1.73×10^6	1.97×10^8	2.10×10^7	–	6.25×10^7	2.21×10^6	8.36×10^5	0.049
5.0	0.0002	5.34×10^5	6.63×10^7	4.00×10^6	–	1.81×10^7	6.09×10^5	4.28×10^5	0.057
8.0	0.0002	2.15×10^5	2.76×10^7	1.18×10^6	–	5.62×10^6	–	–	–
0.8	0.001	4.11×10^7	1.44×10^{10}	1.83×10^9	2.01×10^6	9.97×10^7	1.31×10^7	3.83×10^5	0.135
0.9	0.001	2.91×10^7	9.15×10^9	1.42×10^9	2.03×10^6	9.11×10^7	1.34×10^7	1.15×10^6	0.160
1.0	0.001	2.27×10^7	6.11×10^9	1.15×10^9	2.62×10^6	1.00×10^8	1.09×10^7	1.40×10^6	0.123
1.2	0.001	1.76×10^7	3.04×10^9	7.98×10^8	2.82×10^6	9.18×10^7	1.10×10^7	1.71×10^6	0.138
1.5	0.001	1.10×10^7	1.35×10^9	4.67×10^8	3.63×10^6	9.21×10^7	1.01×10^7	1.77×10^6	0.129
2.0	0.001	4.34×10^6	6.38×10^8	1.12×10^8	1.59×10^6	9.88×10^7	8.09×10^6	1.71×10^6	0.099
3.0	0.001	1.69×10^6	2.13×10^8	2.15×10^7	–	7.66×10^7	2.94×10^6	7.90×10^5	0.049
5.0	0.001	5.81×10^5	7.21×10^7	2.95×10^6	–	1.88×10^7	6.14×10^5	3.60×10^5	0.052
8.0	0.001	2.29×10^5	2.92×10^7	7.75×10^5	–	5.68×10^6	–	–	–
0.85	0.004	4.55×10^7	1.35×10^{10}	2.33×10^9	2.06×10^6	1.03×10^8	1.47×10^7	5.70×10^5	0.148
0.9	0.004	3.85×10^7	1.07×10^{10}	2.11×10^9	2.36×10^6	1.06×10^8	1.34×10^7	7.22×10^5	0.133
1.0	0.004	2.92×10^7	6.98×10^9	1.73×10^9	2.18×10^6	1.02×10^8	1.30×10^7	9.23×10^5	0.136
1.2	0.004	1.82×10^7	3.35×10^9	1.17×10^9	2.98×10^6	1.04×10^8	1.15×10^7	1.01×10^6	0.120
1.5	0.004	1.71×10^7	1.60×10^9	5.06×10^8	3.25×10^6	1.02×10^8	1.09×10^7	1.18×10^6	0.118
2.0	0.004	1.04×10^7	6.80×10^8	1.48×10^8	3.26×10^6	1.11×10^8	1.13×10^7	1.87×10^6	0.119
3.0	0.004	2.18×10^6	2.36×10^8	2.21×10^7	–	1.06×10^8	4.74×10^6	8.39×10^5	0.053
5.0	0.004	1.14×10^6	7.08×10^7	4.50×10^6	–	2.36×10^7	9.41×10^5	3.36×10^5	0.054
8.0	0.004	2.56×10^5	3.02×10^7	6.85×10^5	–	6.57×10^6	–	–	–
1.0	0.01	4.03×10^7	8.92×10^9	2.34×10^9	2.96×10^6	1.09×10^8	1.47×10^7	4.53×10^5	0.139
1.2	0.01	2.58×10^7	4.26×10^9	1.47×10^9	3.13×10^6	1.26×10^8	1.04×10^7	4.61×10^5	0.086
1.5	0.01	2.26×10^7	1.99×10^9	6.11×10^8	3.33×10^6	1.11×10^8	1.27×10^7	5.07×10^5	0.119
2.0	0.01	1.67×10^7	8.39×10^8	1.67×10^8	3.79×10^6	1.20×10^8	1.34×10^7	1.21×10^6	0.122
3.0	0.01	5.59×10^6	2.77×10^8	3.20×10^7	–	1.35×10^8	7.32×10^6	1.17×10^6	0.063
5.0	0.01	1.46×10^6	7.89×10^7	4.18×10^6	–	2.73×10^7	1.27×10^6	1.86×10^5	0.053
8.0	0.01	4.54×10^5	2.95×10^7	9.80×10^5	–	7.70×10^6	–	–	–
1.0	0.02	5.01×10^7	1.09×10^{10}	2.94×10^9	2.30×10^6	1.17×10^8	1.61×10^7	1.52×10^5	0.139
1.2	0.02	2.98×10^7	5.10×10^9	1.86×10^9	2.52×10^6	1.20×10^8	1.43×10^7	1.49×10^5	0.120
1.5	0.02	1.63×10^7	2.37×10^9	7.43×10^8	2.36×10^6	1.10×10^8	1.54×10^7	2.04×10^5	0.142
2.0	0.02	2.42×10^7	9.74×10^8	1.62×10^8	2.96×10^6	1.24×10^8	1.50×10^7	9.40×10^5	0.129
3.0	0.02	8.68×10^6	2.86×10^8	2.90×10^7	–	1.75×10^8	1.31×10^7	1.33×10^6	0.082
5.0	0.02	2.07×10^6	7.49×10^7	5.66×10^6	–	3.32×10^7	1.77×10^6	1.16×10^5	0.057
8.0	0.02	5.51×10^5	2.69×10^7	1.35×10^6	–	1.03×10^7	3.07×10^5	3.29×10^5	0.062
1.0	0.05	5.27×10^7	1.07×10^{10}	3.52×10^9	2.71×10^6	1.24×10^8	1.79×10^7	———	0.144
1.2	0.05	3.18×10^7	5.05×10^9	2.10×10^9	2.64×10^6	1.28×10^8	1.46×10^7	———	0.114
1.5	0.05	1.79×10^7	2.30×10^9	8.12×10^8	2.77×10^6	1.29×10^8	1.37×10^7	2.61×10^4	0.106
2.0	0.05	4.11×10^7	9.25×10^8	1.85×10^8	1.30×10^6	1.64×10^8	1.26×10^7	———	0.077
3.0	0.05	1.14×10^7	2.65×10^8	2.88×10^7	–	1.60×10^8	1.34×10^7	2.35×10^4	0.084
5.0	0.05	2.35×10^6	6.39×10^7	5.25×10^6	–	3.10×10^7	2.29×10^6	1.47×10^4	0.074
8.0	0.05	6.10×10^5	2.14×10^7	1.07×10^6	–	7.22×10^6	6.61×10^5	6.65×10^4	0.101
0.8	0.1	4.00×10^7	7.37×10^9	3.01×10^9	3.52×10^6	1.08×10^8	1.28×10^7	———	0.118
0.9	0.1	3.07×10^7	4.74×10^9	2.10×10^9	3.01×10^6	1.00×10^8	6.54×10^6	———	0.065
1.0	0.1	2.36×10^7	3.28×10^9	1.39×10^9	3.35×10^6	9.71×10^7	4.91×10^6	———	0.051
1.2	0.1	1.57×10^7	1.82×10^9	6.34×10^8	1.82×10^6	1.09×10^8	3.46×10^6	———	0.032

with convective overshoot producing larger cores during MS evolution. The question of the degree of convective mixing during core helium burning due to processes such as breathing pulses and convective overshoot can be addressed by comparing relative numbers of AGB stars and HB stars in globular clusters (e.g. Caputo et al. 1989). For the well-studied cluster M5, this ratio N(AGB)/N(HB) = 0.147 ± 0.026 (Buonanno, Corsi & Fusi Pecci 1981; Brocato, Castellani & Ripepi 1995) is consistent with our theoretical value

Table 1 – *continued*

$M/\mathrm{M}_\odot$	Z	τ_{PMS} (yr)	τ_{MS} (yr)	τ_{CHeI} (yr)	τ_{CHeF} (yr)	τ_{CHeB} (yr)	τ_{EAGB} (yr)	τ_{TAGB} (yr)	$\tau_{\mathrm{AGB}}/\tau_{\mathrm{CHeB}}$
1.5	0.1	5.14×10^7	8.78×10^8	2.13×10^8	2.60×10^6	1.23×10^8	4.05×10^6	———	0.033
2.0	0.1	2.02×10^7	3.58×10^8	4.48×10^7	–	1.26×10^8	3.70×10^6	———	0.029
3.0	0.1	4.77×10^6	1.04×10^8	1.20×10^7	–	4.40×10^7	2.62×10^6	———	0.060
5.0	0.1	1.12×10^6	2.45×10^7	2.67×10^6	–	1.04×10^7	1.23×10^6	———	0.118
8.0	0.1	2.61×10^5	9.39×10^6	3.30×10^5	–	3.48×10^6	2.64×10^5	———	0.076

——— indicates that there is no TPAGB phase.

Table 2. Mass limits for the TPAGB to occur.

Z	$M_{\mathrm{flo1}}/\mathrm{M}_\odot$	$M_{\mathrm{flo2}}/\mathrm{M}_\odot$	$M_{\mathrm{fup}}/\mathrm{M}_\odot$	$M_{\mathrm{cc}}/\mathrm{M}_\odot$
0.0002	0.83	0.83	10	6.5
0.001	0.86	0.87	11	7.5
0.004	0.90	0.94	11	7.5
0.01	0.97	1.09	11.5	8.0
0.02	1.03	1.50	12.0	9.0
0.05	1.42	–	13.0	9.5
0.10	–	–	–	7.5

for stars of masses and heavy element abundance relevant to this cluster.

4 THERMAL PULSE PROPERTIES

Helium shell flashes will occur in stars whose initial mass lies in a certain range M_{flo}–M_{fup} that depends on heavy element abundance. An upper bound on the upper limit, M_{fup}, is set by the requirement that thermal pulses begin before core collapse. For models which have $Z \leqslant 0.02$, the lower limit, M_{flo}, is set by the requirement that the star can evolve to the thermal pulse phase in the time since its formation. To determine M_{flo} for this case, we assume that age of the Universe is 13.7 Gyr (Spergel et al. 2003) and that the first stars take 0.25 Gyr to form (Kogut et al. 2003). Since heavy element abundance-age determinations of F and G MS stars in the Galactic disc show a large scatter (Edvardsson et al. 1993; Reddy et al. 2003), there is probably no simple relation between heavy element abundance and age for stars in the Galaxy, and so we consider two simple models for the way heavy element abundance increases with time in the Galaxy that might be representative of some components of the Galaxy. In the first model, we assume a rapid initial increase in heavy element abundance with no further enrichment, and in the second model we assume that heavy element abundance increases linearly with time with solar abundance reached when the Galaxy is 8.3-Gyr old. For the higher heavy element abundance models, M_{flo} is set by the requirement that mass loss does not remove the envelope before the thermal pulse stage. Indeed for stars with $Z = 0.1$ and initial masses between 0.8 and 3.0 $\mathrm{M}_\odot$, we find there is no thermally pulsing AGB (TPAGB). However, some of these models do experience VLTPs. In Table 2, we show the mass range limits as a function of heavy element abundance. Here M_{cc} is the minimum initial mass for which we find that carbon burning occurs, and M_{fup} is the highest initial mass for which we find helium shell flashes occur. As previously shown by Ritossa, García-Berro & Iben (1996), helium shell flashes can occur after core carbon burning and so M_{fup} is greater than M_{cc}.

In Table 3, we give the number of AGB thermal pulses, N, the mean interval between thermal pulses, $\overline{\Delta t}$, and the minimum interval between thermal pulses, Δt_{min}. As was original found by Paczynski (1974), $\overline{\Delta t}$ decreases with increasing core mass. At a fixed value of the core mass, we find that $\overline{\Delta t}$ decreases also with increasing Z. Since core masses are generally smaller during the TPAGB for stars with higher Z and the same initial mass, this leads to the mean

Table 3. Number of AGB thermal pulses, mean and minimum interval between pulses, mean value of the TDU parameter.

Z	$M/\mathrm{M}_\odot$	N	$\overline{\Delta t}$ (yr)	Δt_{min} (yr)	$\bar{\lambda}$
0.0002	0.9	7	2.2×10^5	1.2×10^5	0.0037
	1.0	10	1.9×10^5	1.0×10^5	0.023
	1.2	19	1.2×10^5	5.3×10^4	0.016
	1.5	34	6.8×10^4	2.4×10^4	0.0091
	2.0	65	2.8×10^4	8.6×10^3	0.013
	3.0	232	3.6×10^3	1.6×10^3	0.048
	5.0	1505	2.9×10^2	1.8×10^2	0.41
0.001	0.9	5	2.3×10^5	1.9×10^5	0.0012
	1.0	8	1.8×10^5	1.1×10^5	0.040
	1.2	12	1.4×10^5	7.8×10^4	0.047
	1.5	19	1.1×10^5	5.0×10^4	0.019
	2.0	31	5.7×10^4	2.3×10^4	0.019
	3.0	81	1.0×10^4	5.0×10^3	0.033
	5.0	406	8.9×10^2	7.4×10^2	0.11
0.004	0.9	4	1.8×10^5	1.7×10^5	–
	1.0	5	1.7×10^5	1.7×10^5	–
	1.2	7	1.5×10^5	8.2×10^4	0.002
	1.5	9	1.3×10^5	9.5×10^4	0.037
	2.0	18	1.2×10^5	5.8×10^4	0.011
	3.0	29	2.9×10^4	1.8×10^4	0.016
	5.0	127	2.7×10^3	1.9×10^3	0.067
0.01	0.95	3	1.3×10^5	1.3×10^5	–
	1.0	4	1.2×10^5	1.1×10^5	–
	1.2	5	1.0×10^5	7.7×10^4	–
	1.5	5	1.1×10^5	8.0×10^4	–
	2.0	13	9.8×10^4	5.8×10^4	0.0026
	3.0	24	4.5×10^4	1.6×10^4	0.026
	5.0	45	4.2×10^3	3.8×10^3	0.050
	8.0	>253	3.8×10^2	–	0.16
0.02	1.0	2	9.4×10^4	8.3×10^4	–
	1.2	2	8.5×10^4	7.9×10^4	–
	1.5	4	1.1×10^5	1.0×10^5	–
	2.0	10	1.0×10^5	8.4×10^4	–
	2.5	18	9.3×10^4	6.1×10^4	0.0016
	3.0	21	6.6×10^4	3.7×10^4	0.0057
	5.0	19	6.4×10^3	6.2×10^3	0.025
	6.5	58	2.4×10^3	2.0×10^3	0.066
	8.0	46	5.2×10^2	4.5×10^2	0.12
0.05	3.0	2	1.2×10^4	1.2×10^4	–
	5.0	3	6.1×10^3	5.9×10^3	–
	8.0	55	1.2×10^3	1.2×10^3	0.054

interval between pulses depending mainly on the initial stellar mass and only weakly on the heavy element abundance. Because stars with lower heavy element abundances are smaller, they have lower mass-loss rates and therefore experience more thermal pulses.

Of fundamental interest to explain the carbon star luminosity function of the Magellanic Clouds is the degree of third dredge-up (TDU) following a helium shell flash. This is quantified by the parameter (e.g. Boothroyd & Sackmann 1988)

$$\lambda = \frac{\Delta M_{\rm dredge}}{\Delta M_{\rm core}}, \tag{8}$$

where $\Delta M_{\rm dredge}$ is the mass dredged-up by the convective envelope and $\Delta M_{\rm core}$ is the amount by which the hydrogen-exhausted core mass increases due to H-burning during the preceding interpulse period. In principle, the value of λ should depend only on physical parameters, such as the heavy element abundance, the core mass and possibly the total stellar mass. However, the amount of TDU found in evolutionary calculations is found to depend also on the numerical treatment of convection (Frost & Lattanzio 1996) and the composition equations (Pols & Tout 2001). Some codes do not find any TDU for low-mass stars unless convective overshoot is included (Herwig et al. 1997; Mowlavi 1999), whereas Pols & Tout (2001), Karakas, Lattanzio & Pols (2002) and Stancliffe, Izzard & Tout (2005) find very efficient dredge-up with $\lambda \sim 1$. Pols & Tout (2001) and Stancliffe et al. (2005) emphasize that the codes that find efficient TDU without using overshoot solve the composition equations simultaneously with the structure equations. The physical importance of this is that opacity and energy changes associated with changing composition are properly accounted for. However, more work is needed to clarify the significance of this for TDU calculations. We give the mean values of λ for our calculations in the last column of Table 3. We find only modest amounts of dredge-up but λ does follow the trends found by Boothroyd & Sackmann (1988), i.e. it increases with decreasing Z and increasing mass. Significantly, we do not find the very efficient dredge-up of Pols & Tout (2001), Karakas et al. (2002) and Stancliffe et al. (2005) even though we solve the structure and composition equations simultaneously. Hence, it is likely that the contrary TDU behaviour is due to different treatments of the finite differencing of the convective diffusion coefficient.

Due to our small values for λ, only the 3 $M_\odot$ models with $Z = 0.0002$ and 0.001 become carbon stars after 40 and 79 pulses, respectively. At higher Z values, mass loss removes the envelope before a sufficient number of pulses have occurred to produce a carbon star. To obtain consistency with the Magellanic Clouds', carbon star luminosity functions require significantly higher values for λ (Marigo, Girardi & Bressan 1999) and/or more thermal pulses. Although our 5 $M_\odot$ $Z = 0.0002$ and 0.001 models experience large numbers of pulses with higher λ, they do not produce carbon stars because most of the dredged-up carbon is destroyed by hot bottom burning (Iben 1975; Lattanzio et al. 1996).

5 INITIAL MASS–FINAL MASS RELATION

We give in Table 4 the final white dwarf mass, $M_{\rm f}$, for a range of initial masses and heavy element abundances. Numbers in italics are the mass of the hydrogen-exhausted core at the time when the envelope becomes unstable. Our results for $Z = 0.02$ agree with the semi-empirical $M_{\rm i}$–$M_{\rm f}$ relation (Weidemann 2000, and references therein). We show in Fig. 3 our $M_{\rm i}$–$M_{\rm f}$ relation and the observational data. Error bars are shown for the Pleiades white dwarf LB1497. These errors are representative of the absolute error in white dwarf mass and the relative error in the progenitor mass. Although we have not applied our models to determine the cluster ages, we find the good agreement between our theoretical $M_{\rm i}$–$M_{\rm f}$ relation and the semi-empirical $M_{\rm i}$–$M_{\rm f}$ relation encouraging in that it indicates that our neglect of mixing by convective overshoot and our specific treatment of mass loss are reasonable.

Table 4. Final white dwarf mass.

$M_{\rm init}/{\rm M}_\odot$	Z						
	0.0002	0.001	0.004	0.01	0.02	0.05	0.10
0.80							0.569
0.85	0.575						
0.90	0.593	0.574	0.550				0.640
0.95				0.545			
1.00	0.633	0.603	0.567	0.545	0.541	0.539	0.693
1.20	0.700	0.643	0.586	0.569	0.557	0.553	0.744
1.50	0.775	0.692	0.617	0.586	0.563	0.569	0.733
2.00	0.869	0.766	0.667	0.632	0.595	0.596	0.741
2.50					0.632	0.627	
3.00	1.054	0.933	0.792	0.730	0.678	0.661	0.794
4.00					0.778		
5.00	1.23	1.11	0.998	0.941	0.874	0.830	0.898
6.50					0.973		
8.00					1.08	0.986	
10.0					1.11	1.20	

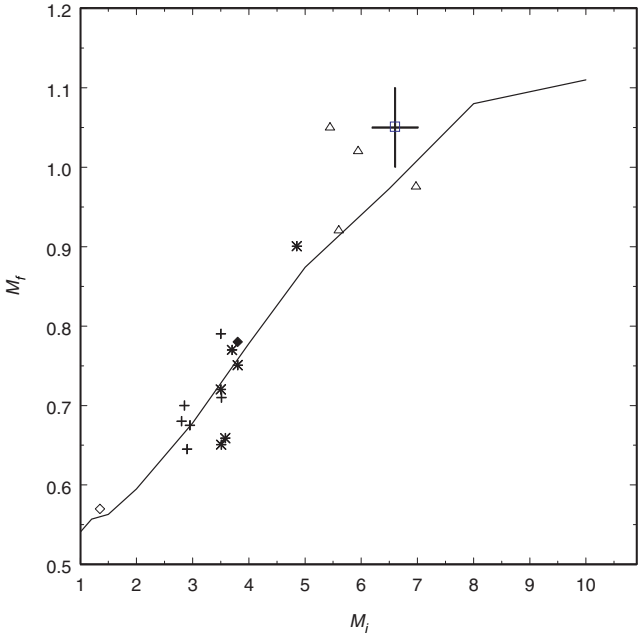

Figure 3. The initial mass–final mass ($M_{\rm i}$ –$M_{\rm f}$) relation for $Z = 0.02$. Also shown are the observational data for M67 (◇), the Hyades (+), NGC 3532 (∗), PG0922 (♦), NGC 2516 (△) and the Pleiades (□). Error bars are shown for the Pleiades white dwarf. These errors are representative of the absolute error in $M_{\rm f}$ and the relative error in $M_{\rm i}$.

6 WHITE DWARF HYDROGEN AND HELIUM LAYER MASSES

In this section, we first describe the different possible paths of post-AGB evolution, followed by consideration of how mass loss affects the ratio of H- and He-burning lifetimes, the relative production of

DA and non-DA white dwarf remnants, and the final mass of helium in a white dwarf star.

6.1 Post-AGB evolution scenarios

As outlined by Iben (1984), the masses of hydrogen- and helium-rich layers in the white dwarf remnant depend on whether the star leaves the AGB-burning hydrogen or helium, and on whether it experiences a final helium shell flash after leaving the AGB. Iben identifies six distinct types of model behaviour.

Type I models leave the AGB during the extended hydrogen-burning phase of a pulse cycle and continue to burn hydrogen during the CSPN phase until the envelope mass drops below a critical value. Significant nuclear energy generation ceases and the star cools as a DA white dwarf.

The evolution of type II models is similar to that of type I models except that a helium shell flash occurs after the star has begun cooling as a white dwarf (Fujimoto 1977; Schönberner 1979). This VLTP causes the star to evolve back to a red giant configuration in what Iben (1984) called BA evolution. Most of the hydrogen in the envelope is engulfed by the convective shell and consumed by nuclear reactions (Iben & MacDonald 1995). During the ensuing quiescent helium-burning phase, winds can strip off any remaining hydrogen containing layers so that the surrounding nebula will be helium-rich and the central star ends up as a non-DA white dwarf (Iben et al. 1983).

Types III and IV models experience a helium shell flash while burning hydrogen after leaving the AGB. This LTP also causes the star to return to the AGB but unlike the type II models hydrogen does not burn. Again winds might strip off all remaining hydrogen to produce a non-DA white dwarf. The distinction between types III and IV models is based on the effective temperature of the star when the helium shell flash occurs. In type III models, the effective temperature is high enough ($T_{\rm e} > 30\,000$ K) to excite a planetary nebula, whereas type IV models are too cool for PN excitation.

Type V models leave the AGB during a helium shell flash and type VI models leave the AGB during quiescent helium burning. During the CSPN phase, they burn helium quiescently and they can become non-DA white dwarfs only if they lose sufficient mass during this phase.

Due to the high AGB mass-loss rates, our models with $Z = 0.05$ and 0.1 can leave the AGB during the EAGB phase before the start of the TPAGB phase. To accommodate this behaviour, we add four new departure types. Type VII models leave the EAGB-burning helium and continue to burn helium quiescently after leaving the AGB. They become white dwarfs once helium-burning reactions die out. The behaviour of type VIII models is similar to that of type VII models except that a final helium shell flash occurs on the white dwarf cooling track. Type IX models leave the AGB during the hydrogen-burning phase that follows after the end of helium burning on the EAGB. They continue to burn hydrogen and become white dwarfs without experiencing a final helium shell flash. Type X models are similar to type IX models except that they experience a final helium shell flash after starting to cool as white dwarfs. Types IX and X models are similar to type I and II models, respectively, except that do not have a TPAGB phase.

In Table 5, we give the AGB departure type for the JM04 tracks. To be specific, we define the point of departure from the AGB to be when the stellar radius has decreased to the value it had at the end of core helium burning, i.e. at the point of arrival on the AGB. This definition gives a departure point that is essentially the same as that found by using Iben's point of greatest variation of radius with hydrogen-rich envelope mass. We use our definition because it is easier to apply. We also give in Table 5, $M_{\rm cs}$ and $M_{\rm es}$, the masses of the hydrogen exhausted core and the hydrogen-rich envelope at the start of the TPAGB, $M_{\rm cd}$ and $M_{\rm ed}$, the corresponding masses at AGB departure and $M_{\rm Hf}$ and $M_{\rm Hef}$, the masses of hydrogen and helium left when all nuclear reactions have ceased.

6.2 Mass loss and the ratio of He- and H-burning lifetimes

Out of the 32 models in Table 5 that reach the TPAGB phase, i.e. most of those with $Z \leqslant 0.05$, we find seven that leave the AGB while burning helium. If the rate at which mass loss and nuclear reactions depleted the envelope was constant over a thermal pulse cycle, we would expect the ratio of the number of stars that leave the AGB-burning helium to the number of stars that leave the AGB-burning hydrogen to be equal to $f_{\rm heh}$, the ratio of the times spent burning helium and hydrogen (determined from whether the helium buffer mass is decreasing or increasing) during a thermal pulse cycle. Since the luminosity is roughly the same in the two burning phases and the energy available from helium burning is about 10 per cent of the energy available from hydrogen burning, $f_{\rm heh} \approx 0.1$, which is less than the ratio from our models.

However, the rate at which mass loss and nuclear reactions deplete the envelope is not constant. During the TPAGB the mass-loss rate, as given by equations (4)–(6), has strong dependences on stellar radius and stellar mass. Unless the stellar mass changes significantly during the TPAGB phase, it is mainly radius changes that modulate the mass-loss rate during a thermal pulse cycle. The rapid energy release from the helium shell flash causes the stellar radius to briefly increase by as much as 50 per cent shortly after peak helium burning. During quiescent helium burning the hydrogen-burning shell is extinguished and as a consequence the radius declines to a minimum of about 70 per cent of the pre-flash value. Once hydrogen burning is re-established the radius increases again to slightly larger than its pre-flash value. Hence, the mass-loss rate, which increases with radius, is largest during the first 5 per cent or so of the flash cycle and smallest in the quiescent helium-burning phase. Because of the very strong dependence on radius, the peak mass-loss rate is a factor of up to 200 greater than the mass-loss rate during the hydrogen-burning phase. Similarly, the minimum mass-loss rate is approximately 10 per cent of the mass-loss rate during the hydrogen-burning phase. The dependence of mass-loss rate on stellar mass becomes important only for stars that have massive envelopes at the start of the TPAGB. A comparison of the $M_{\rm cs}$ and $M_{\rm es}$ values given in Table 5 shows that dependence will be important for stars with $M \gtrsim 1.5\,{\rm M}_{\odot}$ if $Z \leqslant 0.02$.

To illustrate the radius and mass-loss rate behaviour during the TPAGB for a massive star, we plot in Fig. 4 these quantities against time for the $Z = 0.004, M = 3\,{\rm M}_{\odot}$ model. In Fig. 5, we plot the same quantities but only show the final four thermal pulse cycles. We see that the mass-loss behaviour for the last cycle differs significantly from the previous cycles. During the last cycle, the mass-loss rate in the hydrogen-burning phase is much closer to the peak mass-loss rate during the helium-burning phases than for the earlier thermal pulse cycles. This has a significant impact on the ratio of envelope depletion during the two burning phases. Note that the straight-line segment in the mass-loss rate that appears between the last two flashes is due to the change in mass-loss rate dependence on pulsation period at 620 d. In Fig. 6, we plot the fraction of envelope depletion that occurs during helium burning against pulse cycle. We see that this fraction increases with pulse cycle to a

Table 5. AGB departure type, core and envelope masses at the beginning and end of the TPAGB, and final hydrogen and helium masses.

Z	$M/\mathrm{M}_\odot$	AGB departure type	$M_{\rm cs}/\mathrm{M}_\odot$	$M_{\rm es}/\mathrm{M}_\odot$	$M_{\rm cd}/\mathrm{M}_\odot$	$M_{\rm ed}/\mathrm{M}_\odot$	$M_{\rm Hf}/\mathrm{M}_\odot$	$M_{\rm Hef}/\mathrm{M}_\odot$	$P_{\rm He}$
0.0002	0.9	I	0.5376	0.2101	0.5939	1.43×10^{-3}	1.25×10^{-4}	1.58×10^{-2}	0.12 ± 0.03
	1.0	III	0.5446	0.3206	0.6349	1.07×10^{-3}	1.29×10^{-15}	6.5×10^{-3}	0.11 ± 0.01
	1.2	I	0.5562	0.5385	0.6990	7.12×10^{-4}	6.42×10^{-5}	7.0×10^{-3}	0.15
	1.5	I	0.5815	0.8607	0.7750	4.00×10^{-4}	3.79×10^{-5}	5.1×10^{-3}	0.17
	2.0	I	0.6336	1.3176	0.8691	2.09×10^{-4}	1.94×10^{-5}	1.4×10^{-3}	0.15
	3.0	I	0.8197	2.1423	1.0542	4.4×10^{-5}	5.22×10^{-6}	$6. \times 10^{-4}$	0.12
0.001	0.9	III	0.5337	0.1667	0.5752	1.34×10^{-3}	1.11×10^{-4}	1.13×10^{-2}	0.11 ± 0.03
	1.0	II	0.5428	0.2848	0.6060	9.33×10^{-4}	6.20×10^{-15}	7.7×10^{-3}	0.13 ± 0.04
	1.2	V	0.5488	0.5160	0.6446	8.14×10^{-4}	1.03×10^{-15}	6.1×10^{-3}	0.18
	1.5	I	0.5652	0.8305	0.6922	3.75×10^{-4}	4.29×10^{-5}	5.8×10^{-3}	0.26
	2.0	VI	0.5954	1.3361	0.7663	3.91×10^{-4}	2.80×10^{-5}	2.5×10^{-3}	0.26
	3.0	I	0.7648	2.1822	0.9328	5.19×10^{-5}	7.80×10^{-6}	1.0×10^{-3}	0.18
0.004	0.9	II	0.5286	0.1067	0.5498	1.22×10^{-3}	7.55×10^{-10}	1.33×10^{-2}	0.14 ± 0.03
	1.0	I	0.5339	0.2423	0.5666	1.23×10^{-3}	1.20×10^{-4}	1.43×10^{-2}	0.24 ± 0.09
	1.2	I	0.5434	0.4843	0.5877	8.10×10^{-4}	9.92×10^{-5}	1.40×10^{-2}	0.21 ± 0.12
	1.5	IV	0.5524	0.8169	0.6169	5.59×10^{-4}	2.81×10^{-15}	7.4×10^{-3}	0.16
	2.0	I	0.5474	1.3839	0.6688	3.06×10^{-4}	4.04×10^{-5}	7.8×10^{-3}	0.21
	3.0	I	0.6709	2.2854	0.7920	8.42×10^{-5}	1.55×10^{-5}	4.3×10^{-3}	0.17
0.01	0.95	VI	0.5359	0.0491	0.5433	2.54×10^{-3}	1.14×10^{-4}	1.77×10^{-2}	0.30 ± 0.32
	1.0	V	0.5309	0.1730	0.5446	1.49×10^{-3}	1.18×10^{-4}	1.56×10^{-2}	0.19 ± 0.06
	1.2	I	0.5473	0.4311	0.5682	9.97×10^{-4}	9.54×10^{-5}	1.39×10^{-2}	0.22 ± 0.20
	1.5	VI	0.5578	0.7666	0.5882	6.49×10^{-4}	8.64×10^{-5}	1.11×10^{-2}	0.24 ± 0.15
	2.0	I	0.5519	1.3539	0.6317	3.94×10^{-4}	5.43×10^{-5}	8.6×10^{-3}	0.08
	3.0	III	0.5985	2.3660	0.7232	8.50×10^{-5}	2.18×10^{-16}	2.9×10^{-3}	0.22
0.02	1.0	VI	0.5368	0.0166	0.5397	1.87×10^{-3}	9.60×10^{-5}	1.79×10^{-2}	–
	1.2	VI	0.5508	0.2912	0.5567	1.30×10^{-3}	8.46×10^{-5}	1.60×10^{-2}	–
	1.5	I	0.5534	0.7749	0.5638	8.36×10^{-4}	7.89×10^{-5}	1.43×10^{-2}	0.15 ± 0.14
	2.0	I	0.5434	1.3553	0.5945	4.46×10^{-4}	6.33×10^{-5}	1.02×10^{-2}	0.06
	2.5	II	0.5335	1.9241	0.6339	2.66×10^{-4}	9.84×10^{-16}	5.8×10^{-3}	0.09
	3.0	I	0.5614	2.4048	0.6780	1.57×10^{-4}	2.81×10^{-5}	5.6×10^{-3}	0.07
0.05	1.2	IX	–	–	–	2.20×10^{-3}	5.97×10^{-5}	2.45×10^{-2}	–
	1.5	I	0.5675	0.0265	0.5684	1.30×10^{-3}	5.24×10^{-5}	1.90×10^{-2}	–
	2.0	X	–	–	–	4.06×10^{-4}	1.03×10^{-6}	1.30×10^{-2}	–
	2.5	I	0.6254	0.0068	0.6268	2.92×10^{-4}	3.23×10^{-5}	1.07×10^{-2}	–
	3.0	I	0.6550	1.3743	0.6606	1.59×10^{-4}	2.44×10^{-5}	7.3×10^{-3}	0.08
0.10	0.8	VII	–	–	–	4.55×10^{-3}	2.61×10^{-5}	2.40×10^{-2}	–
	0.9	VIII	–	–	–	1.57×10^{-3}	3.99×10^{-15}	9.9×10^{-3}	–
	1.0	VIII	–	–	–	2.12×10^{-3}	2.40×10^{-15}	9.3×10^{-3}	–
	1.2	VIII	–	–	–	1.85×10^{-4}	4.00×10^{-15}	7.0×10^{-3}	–
	1.5	VIII	–	–	–	5.92×10^{-4}	4.95×10^{-15}	7.6×10^{-3}	–
	2.0	VIII	–	–	–	2.09×10^{-4}	5.11×10^{-15}	7.2×10^{-3}	–
	3.0	VIII	–	–	–	4.79×10^{-4}	1.81×10^{-16}	4.4×10^{-3}	–

maximum of about 0.57 and then decreases over the last few cycles to 0.17. The reason for this behaviour is that most of the mass loss occurs during the last few cycles. For the specific case of the $Z = 0.004, M = 3\,\mathrm{M}_\odot$ model, 1.2 $\mathrm{M}_\odot$ is lost during the final AGB thermal pulse cycle. Because the mass-loss rate has an inverse dependence on stellar mass, the mass-loss rate increases significantly as the final AGB thermal pulse cycle proceeds through the quiescent helium- and hydrogen-burning phases, and since the hydrogen-burning phase follows the quiescent helium-burning phase, the mass lost in the hydrogen-burning phase (1.0 $\mathrm{M}_\odot$) is much larger than the mass lost in the helium-burning phases (0.2 $\mathrm{M}_\odot$). In earlier thermal pulse cycles, the total mass lost is insufficient for the mass dependence of mass-loss rate to be an important effect, and the changes in mass-loss rate are dominated by the effects of radius changes.

For the more massive stars, it is the mass-loss history in the final AGB pulse cycle that determines the probability that the model leaves the AGB during helium burning, and hence we give this probability, $P_{\rm He} = f_{\rm heh}/(1 + f_{\rm heh})$, in Table 5. For the lower mass stars, the picture is much less clear because we find that there can be large cycle-to-cycle variations in $f_{\rm heh}$. For these models, we give the average of the $P_{\rm He}$ values for each AGB thermal pulse cycle plus

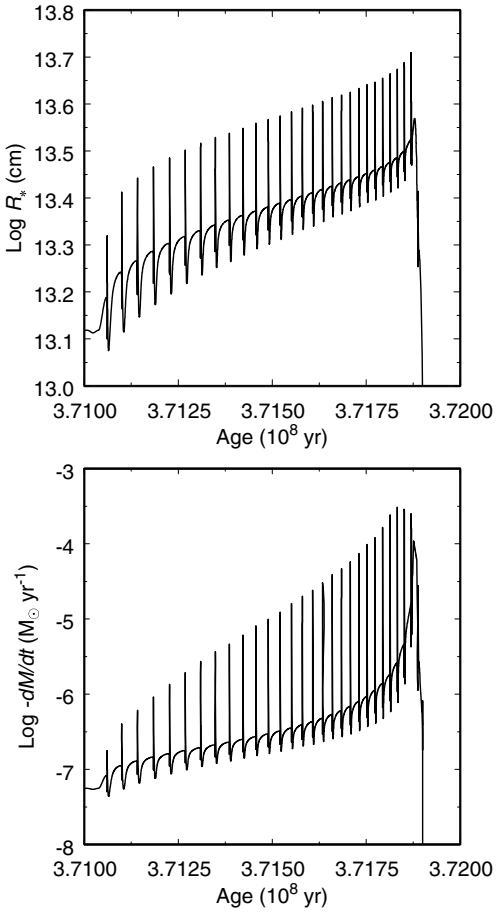

Figure 4. Radius (upper panel) and mass-loss rate (lower panel) during the TPAGB for the $Z = 0.004$, $M = 3\,M_\odot$ model.

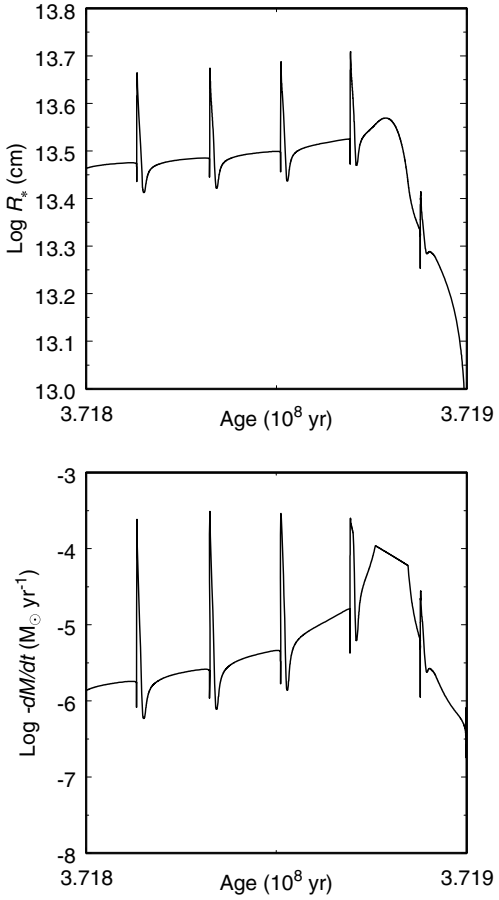

Figure 5. Same as Fig. 4, except that only the final four thermal pulse cycles are shown.

the standard deviation. By averaging the values for $P_{\rm He}$, we estimate that 17 per cent of our models should leave the AGB during helium burning. This estimate is close to the percentage found.

6.3 DA and non-DA white dwarf remnants

Out of the 25 models that leave the TPAGB-burning hydrogen, 19 are type I which become DA white dwarfs, two are type II, three are type III and one is type IV. For the type I models, the amount of hydrogen left on the white dwarf, $M_{\rm Hf}$, increases with Z and decreases with M. If all types II, III and IV models become non-DA white dwarfs at this rate, we would have an inconsistency with the observed non-DA fraction, 1/7, of hot white dwarfs (Sion 1984; Greenstein 1986). Of the six models with types II, III or IV, four end up with a hydrogen mass of the order of 10^{-14} $M_\odot$ or lower, one has a final hydrogen masses of the order of 10^{-9} $M_\odot$ and one has a final hydrogen mass that is similar to those of the type I models. Due to small amounts of numerical diffusion associated with the adaptive mesh, we consider hydrogen masses of the order of 10^{-14} $M_\odot$ to be essentially zero. Hence, roughly 66 per cent of our models with types II, III or IV become non-DA white dwarfs, 17 per cent become thin hydrogen layer DA white dwarfs and 17 per cent become thick hydrogen layer DA white dwarfs. One of the two type V models becomes a non-DA white dwarf, and the five type VI models become thick hydrogen layer DA white dwarfs. Overall we find that 16 per cent of our models become non-DA white dwarfs, 81 per cent become DA white dwarfs with thick ($\sim 10^{-4}$ $M_\odot$) hydrogen layers and 3 per cent become DA white dwarfs with thin ($\sim 10^{-8}\,M_\odot$) hydrogen layers. Given the small number of models considered and other factors such as dependence on heavy element abundance and accretion of hydrogen from the interstellar medium (ISM), our non-DA to DA ratio is in fair agreement with the observed ratio.

6.4 The final mass of helium

To determine limits on $M_{\rm Hef}$ for stars that do not experience a helium flash after leaving the AGB, we plot in Figs 7 and 8 the mass of the helium buffer layer, $M_{\rm buf}$, against core mass, $M_{\rm core}$. Although $M_{\rm Hef}$ differs from $M_{\rm buf}$ because of the presence of heavy elements in the buffer layer, the difference is in general not significant because the amount of TDU is small. Hence, we ignore this difference in determining limits on $M_{\rm Hef}$. We define the buffer layer to be the region between where the hydrogen mass fraction is half its maximum value and where the helium mass fraction is half its maximum value. In Fig. 7, we show the results for all the $3\,M_\odot$ models which have $Z \leqslant 0.02$. In Fig. 8, we show the results for all models of initial mass $\leqslant 5\,M_\odot$ with $Z = 0.001$. It can be seen that, after a few thermal pulse cycles, the star settles down to a state in which the value of $M_{\rm buf}$ at the end of the quiescent helium-burning phase of the thermal pulse cycle is mainly determined by the core mass. The lower envelope of the lines in Fig. 8 provides a lower limit on $M_{\rm Hef}$. To determine an upper limit on $M_{\rm Hef}$, we consider the value of $M_{\rm buf}$ at the end of

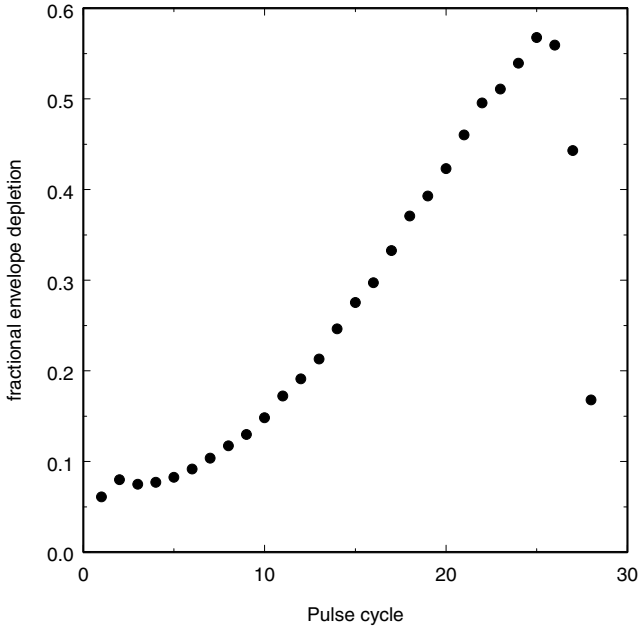

Figure 6. Fraction of envelope depletion that occurs during helium burning against pulse cycle for the $Z = 0.004, M = 3\,\mathrm{M}_\odot$ model.

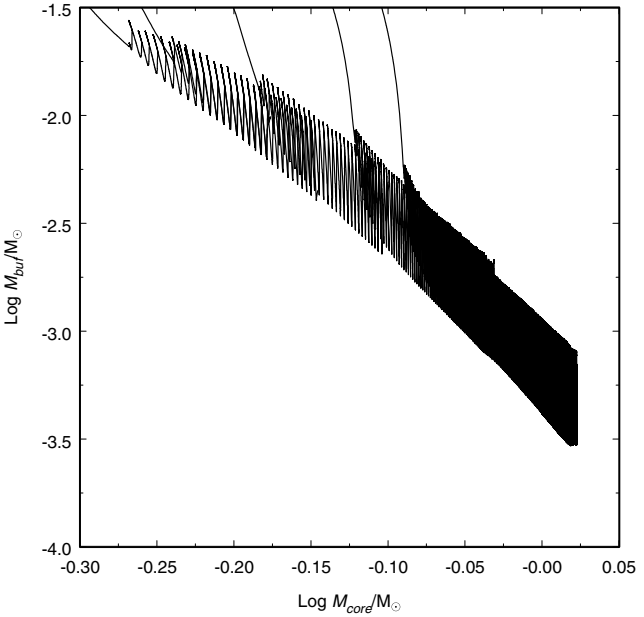

Figure 7. Mass of the helium buffer layer, $M_{\rm buf}$, against core mass, $M_{\rm core}$ for all the 3 $\mathrm{M}_\odot$ models which have $Z \leqslant 0.02$.

the hydrogen-burning phase of the thermal pulse cycle. These limits are well approximated by expressions of the form

$$\log_{10}\left(\frac{M_{\rm buf}}{\mathrm{M}_\odot}\right) = a + b\log_{10}\left(\frac{M_{\rm core}}{\mathrm{M}_\odot}\right) + c\left[\log_{10}\left(\frac{M_{\rm core}}{\mathrm{M}_\odot}\right)\right]^2, \quad \text{for } d \leqslant \frac{M_{\rm core}}{\mathrm{M}_\odot} \leqslant e, \quad (9)$$

where a, b, c, d and e are given in Table 6 for each value of Z. These upper and lower bounds on $M_{\rm buf}$ for $Z = 0.001$ are also shown in Fig. 8.

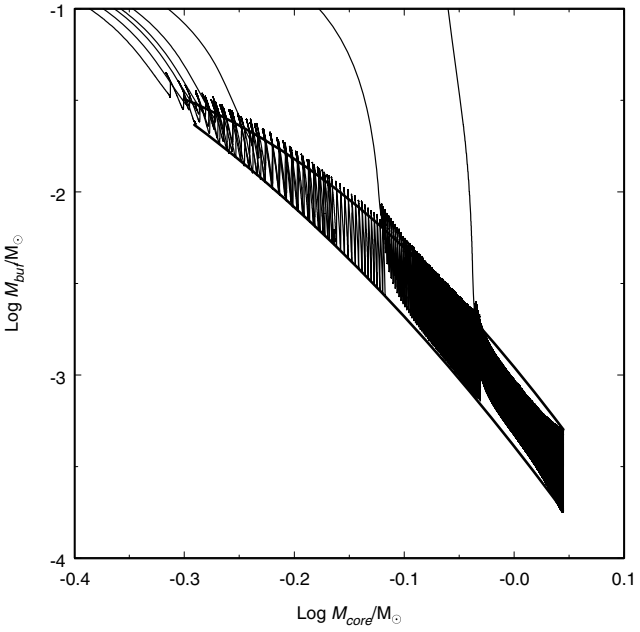

Figure 8. Mass of the helium buffer layer, $M_{\rm buf}$, against core mass, $M_{\rm core}$ for all models of initial mass $\leqslant 5\,\mathrm{M}_\odot$ with $Z = 0.001$. The upper and lower bounds on $M_{\rm buf}$ are also shown by thick solid lines.

The final helium mass is shown in Fig. 9 plotted against white dwarf mass. The different symbols indicate the different heavy element abundances. The general trend is that $M_{\rm Hef}$ decreases with increasing $M_{\rm WD}$. The dependence on Z is weak, with $M_{\rm Hef}$ larger at higher heavy element abundance. In Fig. 10, we plot $M_{\rm Hef}$ against $M_{\rm WD}$ but now the different symbols indicate the different AGB-departure types. The upper and lower bounds on $M_{\rm buf}$, shown in Fig. 8, are also shown in Fig. 10. We see that most of the $M_{\rm Hef}$ values for the type I models lie between these limits and the $M_{\rm Hef}$ values for models that experience helium burning after leaving the AGB are lower than the lower limit for the type I models. As expected, the type VI models, i.e. those that leave the AGB during quiescent helium burning, have $M_{\rm Hef}$ values equal to the lower limit on $M_{\rm buf}$.

For a given $M_{\rm WD}$, the smallest $M_{\rm Hef}$ values occur for types II and III and the largest for the $Z = 0.1$ type VIII models. The type II models experience a helium flash after the star has started to cool as a white dwarf. The flash is caused by compressional heating of the helium layer due to contraction of the non-degenerate outer parts of the core as it cools. Because the core is smaller than on the AGB, a smaller helium layer mass is required to maintain the same pressure and hence $M_{\rm Hef}$ is smaller than for the type I models. However, as can be seen from Fig. 10, the reduction in $M_{\rm Hef}$ is by no more than about 25 per cent. A similar result was found by LM03 for stars of initial mass 1 $\mathrm{M}_\odot$.

7 CRITERIA FOR POST-AGB HELIUM FLASHES

In this section, we determine conditions under which low-mass stars experience a helium flash after leaving the AGB. In a review of helium shell flashes and their consequences, Iben (1987) introduces a parameter

$$\phi = \frac{M_{\rm buf,0}}{\Delta M_{\rm H}}, \quad (10)$$

Table 6. Coefficients in the fits to the lower and upper bounds on buffer mass.

	$M_{\rm buf,min}$					$M_{\rm buf,max}$				
Z	a	b	c	d	e	a	b	c	d	e
0.0002	−3.4083	−8.0814	−7.4303	0.58	1.22	−2.9816	−8.0142	−10.9891	0.57	1.23
0.001	−3.3870	−7.6192	−5.4824	0.51	1.11	−2.8798	−6.3551	−5.5998	0.51	0.93
0.004	−3.3634	−7.4243	−5.1295	0.52	1.00	−2.9293	−7.0296	−7.8623	0.52	1.00
0.01	−3.3243	−6.7603	−3.0043	0.52	0.94	−2.9129	−6.1056	−5.0948	0.52	0.93
0.02	−3.3106	−7.1480	−4.4195	0.51	0.97	−3.0248	−7.5528	−10.5975	0.57	0.97

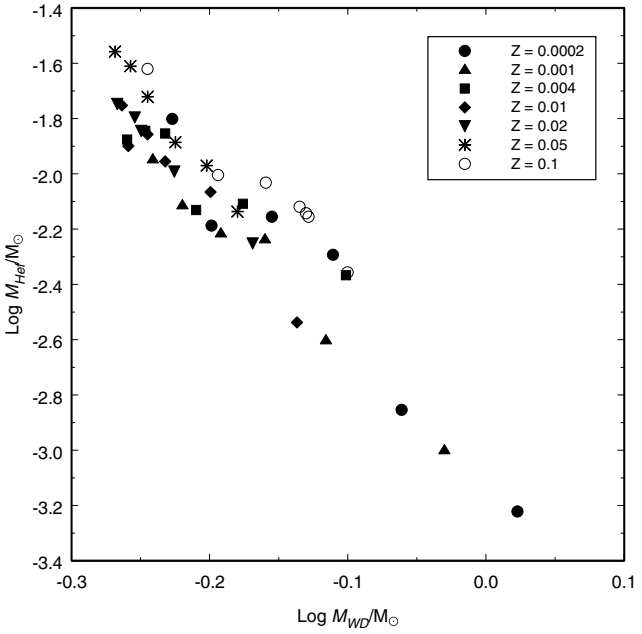

Figure 9. Final helium layer mass, $M_{\rm Hef}$, in solar units plotted against white dwarf mass, $M_{\rm WD}$, in solar units. The different symbols indicate the heavy element abundance.

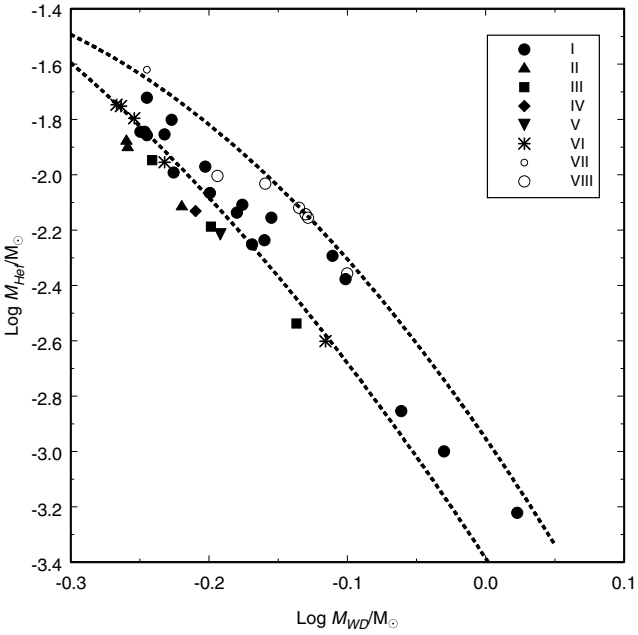

Figure 10. Final helium layer mass, $M_{\rm Hef}$, in solar units plotted against white dwarf mass, $M_{\rm WD}$, in solar units. The symbols indicate AGB-departure type. The upper and lower bounds on $M_{\rm buf}$ are shown by thick broken lines.

where $M_{\rm buf,0}$ is the mass of the helium rich-layer between the hydrogen-burning shell and the carbon-rich layer left behind after the last AGB helium shell flash, and $\Delta M_{\rm H}$ is the mass through which the hydrogen-shell burns in the quiescent hydrogen-burning phase of the thermal pulse cycle. This parameter is a measure of where in the thermal pulse cycle AGB departure occurs, and will be relevant to the onset of post-AGB helium burning provided that the helium layer mass is the main parameter that controls whether helium ignites or not. Based on the computations of Schönberner (1979), Iben et al. (1983) and Iben (1984), Iben (1987) concludes that a post-AGB helium flash will occur after hydrogen burning has ceased (i.e. type II behaviour) if $0.75 < \phi < 0.85$, and a post-AGB helium flash will occur before hydrogen burning has ceased (i.e. type III or IV behaviour) if $0.85 < \phi < 1$.

We find that there are two difficulties in applying Iben's criterion directly to our models. First, about five flash cycles need to occur before $\Delta M_{\rm H}$ remains almost constant from one thermal pulse cycle to the next. For low-mass stars with high heavy element abundances, an insufficient number of complete flash cycles occur before the star leaves the AGB. Secondly, as can be seen from Figs 7 and 8, the minimum and maximum values of $M_{\rm buf}$ in a pulse cycle both decrease as the core grows. Because $M_{\rm buf}$ does not go to zero at the end of the quiescent helium-burning phase, ϕ is not restricted to the range 0–1, and in many cases ϕ exceeds 1. To avoid these difficulties, we modify the definition of ϕ to

$$\phi' = \frac{M_{\rm buf,0} - \overleftrightarrow{M}_{\rm buf,min}}{\overleftrightarrow{M}_{\rm buf,max} - \overleftrightarrow{M}_{\rm buf,min}}, \tag{11}$$

where $\overleftrightarrow{M}_{\rm buf,min}$ and $\overleftrightarrow{M}_{\rm buf,max}$ are obtained by extrapolation of the values of $M_{\rm buf,min}$ and $M_{\rm buf,max}$ for the final two thermal pulse cycles before AGB departure to the point of AGB departure. In Table 7, we give AGB departure type, and the values of $M_{\rm buf,0}$, $\overleftrightarrow{M}_{\rm buf,min}$, $\overleftrightarrow{M}_{\rm buf,max}$, ϕ' and $\Delta M_{\rm H}$ for the last AGB flash cycle. A starred value for ϕ' indicates that the model leaves the AGB-burning helium.

For the type I models, ϕ' ranges from 0.15 to 0.80 with a mean of 0.41. For the two type II models, ϕ' ranges from 0.77 to 0.88 with a mean of 0.83 and for the three type III models, ϕ' ranges from 0.87 to 0.97 with a mean of 0.93. Hence, the trend is in agreement with the findings of Iben (1987) in that type correlates with ϕ'. However, we have too few non-type I models in the JM04 set to be able to determine the values of ϕ' at which transitions in type occur. To do this, we make use of the large number of evolutionary calculations for 1.0 M$_\odot$ stars in the LM03 set. In Table 8, we give the AGB departure

Table 7. Parameters relevant to the criterion for the occurrence of a post-AGB helium shell flash from the JM04 models.

Z	$M/\mathrm{M}_\odot$	AGB departure type	$M_{\mathrm{buf},0}/\mathrm{M}_\odot$	$\overleftrightarrow{M}_{\mathrm{buf,min}}/\mathrm{M}_\odot$	$\overleftrightarrow{M}_{\mathrm{buf,max}}/\mathrm{M}_\odot$	ϕ'	$\Delta M_{\mathrm{H}}/\mathrm{M}_\odot$
0.0002	0.9	I	0.014 94	0.010 02	0.019 78	0.50	0.009 68
	1.0	III	0.015 62	0.007 01	0.015 85	0.97	0.008 94
	1.2	I	0.006 61	0.004 09	0.009 91	0.43	0.006 09
	1.5	I	0.004 89	0.002 17	0.005 90	0.73	0.003 77
	2.0	I	0.001 35	0.001 06	0.002 96	0.15	0.001 98
	3.0	I	0.000 565	0.000 280	0.000 779	0.57	0.000 58
0.001	0.9	III	0.020 38	0.011 13	0.020 72	0.96	0.009 05
	1.0	II	0.015 46	0.008 71	0.017 45	0.77	0.008 89
	1.2	V	0.012 40	0.006 58	0.013 83	0.80*	0.008 10
	1.5	I	0.005 81	0.004 41	0.010 33	0.24	0.005 98
	2.0	VI	0.003 36	0.002 36	0.006 68	0.23*	0.004 15
	3.0	I	0.000 988	0.000 634	0.002 009	0.26	0.001 41
0.004	0.9	II	0.020 13	0.013 98	0.021 00	0.88	0.006 09
	1.0	I	0.013 59	0.012 23	0.020 34	0.17	0.007 81
	1.2	I	0.013 71	0.010 43	0.018 21	0.42	0.008 05
	1.5	IV	0.015 48	0.008 12	0.015 87	0.95	0.008 47
	2.0	I	0.007 90	0.004 81	0.011 61	0.45	0.006 62
	3.0	I	0.004 41	0.001 62	0.005 10	0.80	0.003 28
0.01	0.95	VI	0.020 84	0.020 78	0.024 96	0.01*	0.005 12
	1.0	V	0.016 43	0.014 64	0.022 13	0.24*	0.005 14
	1.2	I	0.013 77	0.011 59	0.015 83	0.51	0.005 09
	1.5	VI	0.012 15	0.010 08	0.016 77	0.31*	0.006 74
	2.0	I	0.008 80	0.006 34	0.011 74	0.46	0.006 67
	3.0	III	0.007 14	0.003 23	0.007 75	0.87	0.004 59
0.02	1.0	VI	0.021 87	0.021 71	0.024 58	0.06*	0.001 92
	1.2	VI	0.020 07	0.019 74	0.022 59	0.12*	–
	1.5	I	0.014 76	0.012 57	0.017 96	0.41	0.004 59
	2.0	I	0.010 45	0.008 93	0.015 11	0.25	0.006 19
	2.5	II	0.011 25	0.006 81	0.012 62	0.76	0.006 02
	3.0	I	0.005 80	0.004 83	0.009 60	0.20	0.005 32

* indicates AGB departure occurs during a helium-burning phase.

Table 8. Parameters relevant to the criterion for the occurrence of a post-AGB helium shell flash from the LM03 models.

Z	AGB departure type	$M_{\mathrm{buf},0}/\mathrm{M}_\odot$	$\overleftrightarrow{M}_{\mathrm{buf,min}}/\mathrm{M}_\odot$	$\overleftrightarrow{M}_{\mathrm{buf,max}}/\mathrm{M}_\odot$	ϕ'
0.001	I	0.0134–0.0110	0.0081	0.0152–0.0156	0.39–0.75
	II	0.0142–0.0134	0.0080–0.0081	0.0151–0.0152	0.75–0.87
	III–IV	0.0142–0.0143	0.0080	0.0150–0.0151	0.87–0.89
0.004	I	0.0149–0.0121	0.0094–0.0096	0.0167–0.0172	0.33–0.75
	II	0.0160–0.0151	0.0094–0.0095	0.0168–0.0169	0.76–0.88
	III–IV	0.0164–0.0159	0.0092–0.0093	0.0168	0.88–0.95
0.010	I	0.0144–0.0120	0.0095–0.0098	0.0165–0.0166	0.36–0.68
	II	0.0156–0.0148	0.0096–0.0098	0.0163–0.0164	0.76–0.89
	III–IV	0.0158–0.0156	0.0096	0.0163–0.0164	0.89–0.93
0.020	I	0.0157–0.0130	0.0112–0.0118	0.0171–0.0177	0.19–0.76
	II	0.0165–0.0158	0.0109–0.0115	0.0171	0.77–0.90
	III–IV	0.0166	0.0109	0.0169–0.0170	0.93–0.95

type, the corresponding ranges of values of $M_{\mathrm{buf},0}$, $\overleftrightarrow{M}_{\mathrm{buf,min}}$, $\overleftrightarrow{M}_{\mathrm{buf,max}}$ and ϕ' for these models. We see that the transition between types II and III occurs at $\phi' \approx 0.88$ which is consistent with the values for the JM04 set in Table 7. The transition between types I and II occurs at $\phi' \approx 0.76$.

8 DISCUSSION

In this section, we first compare our results with the observed abundance patterns of PG1159 stars. We then compare our results for the helium mass with values obtained from asteroseismology and

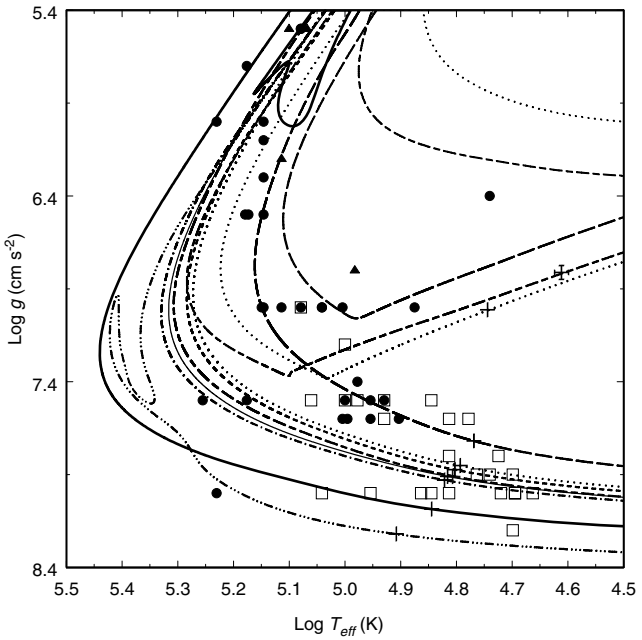

Figure 11. Evolutionary tracks in the $T_{\rm eff}$–g plane for models that produce hydrogen-deficient post-AGB stars. The individual tracks are for $Z = 0.0002$, $M = 1.0\,{\rm M}_{\odot}$ (——), $Z = 0.001$, $M = 1.0\,{\rm M}_{\odot}$ (· · · ·), $Z = 0.001$, $M = 1.2\,{\rm M}_{\odot}$ (·— ·—), $Z = 0.004$, $M = 0.9\,{\rm M}_{\odot}$ (— — —), $Z = 0.004$, $M = 1.5\,{\rm M}_{\odot}$ (— — —), $Z = 0.01$, $M = 3.0\,{\rm M}_{\odot}$ (——), $Z = 0.02$, $M = 2.5\,{\rm M}_{\odot}$ (— — — —) and $Z = 0.1$, $M = 3.0\,{\rm M}_{\odot}$ (—· · ·—). The positions of DO white dwarfs, PG1159 stars and hybrid PG1159 stars are shown by open squares, filled circles and filled triangles, respectively. The plus signs indicate where the model mass-loss rate equals 10^{-13} ${\rm M}_{\odot}$ ${\rm yr}^{-1}$.

analysis of DQ white dwarfs. Finally, we briefly comment on the possibility of self-induced novae.

8.1 Abundances in PG1159 stars

We have not included the effects of element diffusion, gravitational settling and radiative levitation on the composition profile in our calculations. These processes become important once the mass-loss rate drops below a critical value which for white dwarfs is of the order of 10^{-14}–10^{-13} ${\rm M}_{\odot}$ ${\rm yr}^{-1}$ (Michaud 1987; Unglaub & Bues 1998). For our adopted mass-loss algorithm, this value corresponds to a luminosity of the order of 2–10 ${\rm L}_{\odot}$ for solar composition material. In Fig. 11, we show partial tracks in the log $T_{\rm eff}$–log g diagram followed by those of our models that result in helium-dominated atmosphere white dwarfs. Also shown are the spectroscopically determined positions of PG1159 stars (Werner et al. 1997; Dreizler & Heber 1998; Hügelmeyer et al. 2005), DO white dwarfs (Dreizler & Werner 1996; Werner et al. 1997; Hügelmeyer et al. 2005) and hybrid PG1159 stars (Dreizler et al. 1996; Napiwotzki 1999). The point at which the mass-loss rate equals 10^{-13} ${\rm M}_{\odot}$ ${\rm yr}^{-1}$ is also shown for each track. It can be seen that there is considerable overlap between the cooler PG1159 stars and the hotter DO white dwarfs. This indicates that the transition from PG1159 to DO is not simply due to mass-loss rate decreasing with luminosity. Line-radiation driven mass loss is also expected to depend on the amount and distribution of heavy element abundances. In general, we expect that PG1159 stars with lower heavy element abundances to have lower mass-loss rates and hence the transition to DO will occur at higher temperature. Because of these considerations, we will only make abundance comparisons for the PG1159 stars.

In Fig. 12, we show the evolution of the photospheric H/He, C/He, N/He and O/He ratios with log g for the models that lead to He-atmosphere white dwarfs. The initial heavy element abundances for these models range from $Z = 2 \times 10^{-4}$ to 0.1. It can be seen from Fig. 12 that there are differences in abundance evolution, which are in part due to the different mass-loss rates. In general, higher mass remnants have higher CSPN plateau luminosities. These leads to higher mass-loss rates which, coupled with the fact that they have less massive H-rich layers, means that it is easier for high-mass remnants to lose their H-rich envelopes to expose layers processed by helium-burning reactions. The occurrence of a BA flash (AGB departure type II), which produces flash-driven mixing of part of the H-rich envelope into hotter regions where the hydrogen is destroyed, also facilitates the loss of hydrogen. Note that in this figure, results are shown for calculations that did not explicitly include ^{13}C. We have recalculated the VLTPs with ^{13}C explicitly included in the reaction network. However, these calculations give essentially the same results as those in which ^{13}C is assumed to be in equilibrium. The largest effect is that the surface abundance for nitrogen can differ by up to 40 per cent. Differences in the C and O abundances are less than 10 per cent. These points are illustrated by the individual models which we now briefly discuss. The $Z = 0.0002, M = 1.0\,{\rm M}_{\odot}$ model has AGB departure type III, i.e. it left the AGB while burning helium quiescently. Due to earlier dredge-up episodes, the surface abundances of C, N and O at the time of AGB departure have increased to C/He $= 2.4 \times 10^{-3}$, N/He $= 1.1 \times 10^{-4}$ and O/He $= 3.1 \times 10^{-4}$. Due to mass-loss uncovering deeper layers, the C and O abundances rise as the star evolves to the blue. Just before the last vestiges of the H-rich envelope are removed at log $g \approx 6$, there is an increase in the N abundance due to CNO-cycle processing at the bottom of the H-rich envelope. Further, mass loss reduces the N abundance while the C and O abundances continue to increase to their final values at log $g \approx 7$. Similar behaviour is found for the $Z = 0.001, M = 1.2\,{\rm M}_{\odot}$ model which has AGB departure type V, i.e. it left the AGB during the helium shell flash. The $Z = 0.004, M = 1.5\,{\rm M}_{\odot}$ model, which has departure type IV, differs only in that there is no 'bump' in the N abundance at log$g \approx 6$. The $Z = 0.001, M = 1.0\,{\rm M}_{\odot}$ and $Z = 0.02, M = 2.5\,{\rm M}_{\odot}$ models both experience a BA flash (AGB departure type II) that mixes more C and O into the envelope. Hence, these models finally leave the AGB with significantly higher C and O abundances than the non-BA models. Because of the flash-driven mixing of protons into the helium-burning regions where they are destroyed by the ^{12}C $(p, \gamma)^{13}$N reaction, the surface hydrogen abundance drops below H/He $= 1$ at log $g \approx 5$ i.e. at lower gravity than for the types III and V models. As the surface H abundance is further reduced, the N abundance increases. Further mass loss removes all the hydrogen and the final abundances are reached again at log $g \approx 7$. The $Z = 0.004, M = 0.9\,{\rm M}_{\odot}$ model also experiences a BA flash. However, the remnant mass is lower and hence the mass-loss rate is lower and the H-rich envelope is larger for this model than the other two BA models. Mass loss does not remove the entire H-rich envelope and a small amount of H and a significant amount of N is present at log $g \approx 7$. The $Z = 0.01, M = 3.0\,{\rm M}_{\odot}$ model has AGB departure type III, but because its remnant mass is higher than for the $Z = 0.0002, M = 1.0\,{\rm M}_{\odot}$ model, it has a smaller H-rich envelope and higher mass-loss rate after leaving the AGB. The final helium flash causes the star to evolve back towards the red side of the Hertzsprung–Russell diagram (HRD) and most of the hydrogen is removed before the star evolves to the blue for a final time.

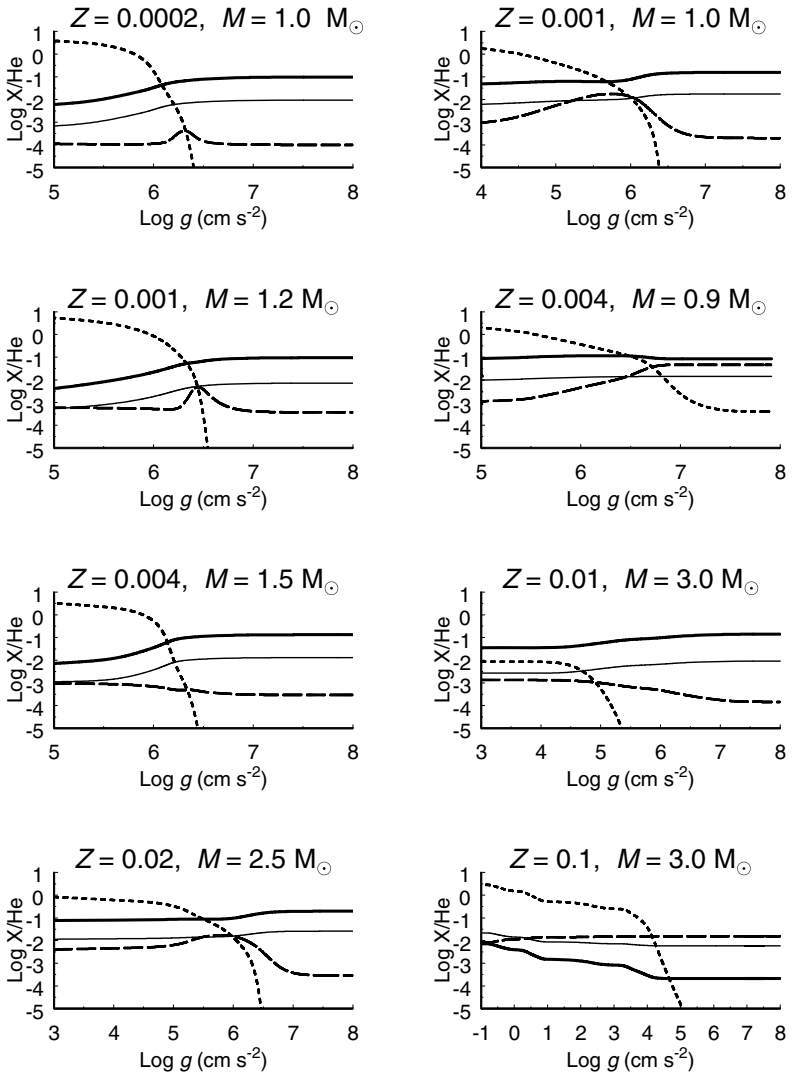

Figure 12. Evolution of the photospheric H/He, C/He, N/He and O/He number ratios with log g for models that lead to helium atmosphere white dwarfs.

To aid comparison with spectroscopically determined abundances, we give in Table 9, the model abundances (number ratios and mass fractions) and the effective temperatures as a function of log g. Note that the model surface abundances do not change significantly for log $g > 7$. Also the C/O ratio remains fairly uniform at $\approx$10 for all models, except for the $Z = 0.1$ model.

The non-local thermodynamic equilibrium (NLTE) spectral analyses of PG1159 stars (Dreizler & Heber 1998; Hügelmeyer et al. 2005) show that the C/He number ratio ranges from 0.01 (SDSS J110215.46+024034.2) to 0.6 (PG1159−035), with clusters around 0.05 and 0.3. The C/O number ratios range from 3 to 10. At log g = 7, the model C/He ratio ranges from about 0.09 to 0.2, with the C/O ratio in the range 6–15. Bearing in mind that the spectral analyses are only able to distinguish between abundance differences of a factor of 2 once log g and $T_{\rm eff}$ have been fixed (Dreizler, private communication; Werner & Herwig 2006), we find that there is considerable overlap between the ranges of observed and model ratios, and agreement is particularly good for some stars, such as MCT0130-1937 (C/He = 0.1, C/O = 10 and log g = 7.5). The oxygen abundance is particularly difficult to pin down because a very detailed treatment of the O VI ion is needed to model the optical lines accurately. Hence, because systematic errors in the C/O abundance ratio cannot be ruled out (Dreizler, private communication), it remains possible that convective overshoot is not necessary to produce the abundances of PG1159 stars. The model Ne abundances, which range from 1 to 2.5 per cent by mass at log g = 7, are consistent with Ne detections in PG1159 stars (Werner et al. 2004).

A few of the PG1159 stars have detectable nitrogen in their atmospheres. Interestingly, all the pulsating PG1159 stars in the sample analysed by Dreizler & Heber (1998) have a N/He ratio of 0.01. The only non-pulsating PG1159 star known to have nitrogen is PG1144+005 (Werner et al. 1997). The presence of N in a C- and O-dominated atmosphere is indicative of BA behaviour (Iben & MacDonald 1995). As can be seen from Table 9, the largest N abundances occur in our models of AGB departure type II. For the other models except the $Z = 0.1$ model, the N abundance is typically two orders of magnitude lower. Again the N abundance at a particular evolutionary stage of the type II models is sensitive to the mass-loss history. If mass loss occurs at too high a rate, then all of the N could be stripped off the star too early at lower gravity than the pulsating PG1159 stars in the Dreizler & Heber sample. If mass loss occurs at too low rate, then too much H could

Table 9. Surface abundances (number ratios and mass fractions) for models that produce a hydrogen-deficient post-AGB star.

				$Z = 0.0002$, $M = 1.0\,M_\odot$, $M_{WD} = 0.633\,M_\odot$, AGB departure type III							
	T_{eff} (kK)	H/He	C/He	N/He	O/He	X(H)	X(He)	X(C)	X(N)	X(O)	X(Ne)
$\log g = 5$	86	3.8	6.0×10^{-3}	1.1×10^{-4}	6.8×10^{-4}	0.484	0.505	0.0091	0.0002	0.0014	0.0004
$\log g = 6$	150	1.8×10^{-1}	3.3×10^{-2}	1.1×10^{-4}	3.5×10^{-3}	0.039	0.859	0.0859	0.0003	0.0123	0.004
$\log g = 7$	210	1.9×10^{-10}	9.3×10^{-2}	1.0×10^{-4}	9.1×10^{-3}	0.000	0.752	0.2115	0.0003	0.0274	0.009
				$Z = 0.001$, $M = 1.0\,M_\odot$, $M_{WD} = 0.603\,M_\odot$, AGB departure type II							
	T_{eff} (kK)	H/He	C/He	N/He	O/He	X(H)	X(He)	X(C)	X(N)	X(O)	X(Ne)
$\log g = 5$	89	4.0×10^{-1}	6.2×10^{-2}	5.4×10^{-3}	8.3×10^{-3}	0.074	0.741	0.138	0.014	0.025	0.007
$\log g = 6$	140	1.2×10^{-2}	7.8×10^{-2}	1.3×10^{-2}	1.1×10^{-2}	0.002	0.747	0.173	0.035	0.033	0.010
$\log g = 7$	190	4.1×10^{-10}	1.5×10^{-1}	2.2×10^{-4}	1.7×10^{-2}	0.000	0.642	0.299	0.0005	0.045	0.013
				$Z = 0.001$, $M = 1.2\,M_\odot$, $M_{WD} = 0.643\,M_\odot$, AGB departure type V							
	T_{eff} (kK)	H/He	C/He	N/He	O/He	X(H)	X(He)	X(C)	X(N)	X(O)	X(Ne)
$\log g = 5$	87	5.2	4.2×10^{-3}	5.8×10^{-4}	5.4×10^{-4}	0.565	0.427	0.005	0.0009	0.0009	0.0004
$\log g = 6$	150	8.5×10^{-1}	2.2×10^{-2}	5.2×10^{-4}	1.8×10^{-3}	0.164	0.775	0.051	0.0014	0.0057	0.002
$\log g = 7$	210	2.8×10^{-10}	9.1×10^{-2}	4.2×10^{-4}	6.9×10^{-3}	0.000	0.761	0.208	0.0011	0.0210	0.009
				$Z = 0.004$, $M = 0.9\,M_\odot$, $M_{WD} = 0.550\,M_\odot$, AGB departure type II							
	T_{eff} (kK)	H/He	C/He	N/He	O/He	X(H)	X(He)	X(C)	X(N)	X(O)	X(Ne)
$\log g = 5$	78	2.0	8.6×10^{-2}	1.1×10^{-3}	9.8×10^{-3}	0.275	0.553	0.143	0.002	0.021	0.005
$\log g = 6$	120	3.6×10^{-1}	1.1×10^{-1}	4.6×10^{-3}	1.3×10^{-2}	0.060	0.660	0.227	0.010	0.034	0.008
$\log g = 7$	140	2.4×10^{-3}	8.5×10^{-2}	4.6×10^{-2}	1.4×10^{-2}	0.000	0.673	0.171	0.108	0.038	0.008
				$Z = 0.004$, $M = 1.5\,M_\odot$, $M_{WD} = 0.617\,M_\odot$, AGB departure type IV							
	T_{eff} (kK)	H/He	C/He	N/He	O/He	X(H)	X(He)	X(C)	X(N)	X(O)	X(Ne)
$\log g = 5$	84	3.3	7.2×10^{-3}	9.5×10^{-4}	1.1×10^{-3}	0.444	0.539	0.012	0.002	0.002	0.0008
$\log g = 6$	140	5.4×10^{-1}	3.5×10^{-2}	6.9×10^{-4}	3.7×10^{-3}	0.106	0.792	0.085	0.002	0.012	0.003
$\log g = 7$	190	5.2×10^{-10}	1.3×10^{-1}	3.0×10^{-4}	1.3×10^{-2}	0.000	0.686	0.268	0.0007	0.035	0.009
				$Z = 0.01$, $M = 3.0\,M_\odot$, $M_{WD} = 0.730\,M_\odot$, AGB departure type III							
	T_{eff}(kK)	H/He	C/He	N/He	O/He	X(H)	X(He)	X(C)	X(N)	X(O)	X(Ne)
$\log g = 5$	100	5.4×10^{-4}	5.8×10^{-2}	1.0×10^{-3}	4.2×10^{-3}	0.000	0.829	0.142	0.003	0.014	0.010
$\log g = 6$	170	5.5×10^{-8}	9.8×10^{-2}	4.7×10^{-4}	6.6×10^{-3}	0.000	0.745	0.218	0.001	0.020	0.014
$\log g = 7$	270	1.3×10^{-11}	1.3×10^{-1}	1.8×10^{-4}	8.7×10^{-3}	0.000	0.682	0.276	0.0004	0.024	0.016
				$Z = 0.02$, $M = 2.5\,M_\odot$, $M_{WD} = 0.632\,M_\odot$, AGB departure type II							
	T_{eff} (kK)	H/He	C/He	N/He	O/He	X(H)	X(He)	X(C)	X(N)	X(O)	X(Ne)
$\log g = 5$	91	3.3×10^{-1}	8.7×10^{-2}	6.3×10^{-3}	1.3×10^{-2}	0.057	0.693	0.180	0.015	0.036	0.015
$\log g = 6$	150	1.3×10^{-2}	9.8×10^{-2}	1.5×10^{-2}	1.6×10^{-2}	0.002	0.693	0.201	0.038	0.044	0.019
$\log g = 7$	200	3.2×10^{-10}	1.9×10^{-1}	3.8×10^{-4}	2.6×10^{-2}	0.000	0.577	0.334	0.0008	0.059	0.025
				$Z = 0.02$, $M = 2.5\,M_\odot$, $M_{WD} = 0.632\,M_\odot$, AGB departure type II, ^{13}C included							
	T_{eff} (kK)	H/He	C/He	N/He	O/He	X(H)	X(He)	X(C)	X(N)	X(O)	X(Ne)
$\log g = 5$	91	3.2×10^{-1}	9.6×10^{-2}	3.8×10^{-3}	1.4×10^{-2}	0.055	0.680	0.197	0.009	0.038	0.017
$\log g = 6$	150	2.2×10^{-2}	1.0×10^{-1}	1.2×10^{-2}	1.6×10^{-2}	0.004	0.688	0.213	0.029	0.043	0.019
$\log g = 7$	200	7.5×10^{-10}	1.8×10^{-1}	5.2×10^{-4}	2.4×10^{-2}	0.000	0.589	0.325	0.0011	0.057	0.025
				$Z = 0.1$, $M = 3.0\,M_\odot$, $M_{WD} = 0.794\,M_\odot$, AGB departure type VIII							
	T_{eff} (kK)	H/He	C/He	N/He	O/He	X(H)	X(He)	X(C)	X(N)	X(O)	X(Ne)
$\log g = 5$	87	1.6×10^{-5}	2.1×10^{-4}	1.5×10^{-2}	5.9×10^{-3}	0.000	0.901	0.0006	0.049	0.021	0.010
$\log g = 6$	150	6.9×10^{-9}	2.1×10^{-4}	1.5×10^{-2}	5.9×10^{-3}	0.000	0.901	0.0006	0.049	0.021	0.010
$\log g = 7$	260	4.4×10^{-12}	2.1×10^{-4}	1.5×10^{-2}	5.9×10^{-3}	0.000	0.901	0.0006	0.049	0.021	0.010

remain in addition to the nitrogen. Table 9 indicates that N/He = 0.01 occurs in the type II models near log $g = 6$ and in two of the three models is reduced to 2–4 $\times$ 10^{-4} by the time that log g = 7. Only in the least massive model with the lowest mass-loss rate is there enough N at log $g = 7$. This comparison suggests that we have used too high a mass-loss rate for the post-AGB phases of the evolution of the two more massive models. However, a reasonable conclusion is that PG1159 stars with detectable N are produced from stars that experience BA behaviour. If the presence of N is a requirement for a PG1159 star to pulsate, then we can conclude that the reason why some PG1159 stars show pulsations and others of similar temperature and gravity do not, is due to a difference in formation channel i.e. the pulsators are descendants of BA stars.

Important objects for understanding the formation of H-deficient atmospheres are the hybrid PG1159 stars. These objects are low-gravity PG1159 stars that show prominent hydrogen Balmer lines (Napiwotzki & Schönberner 1991). Spectral analysis of the well-studied hybrid PG1159 star HS 2324+3944 (Dreizler et al. 1996) gives $T_{\rm eff} = 130\,000 \pm 10\,000$ K, $\log g = 6.2 \pm 0.2$, He/H = $0.5^{+0.2}_{-0.1}$, C/H = 0.15 ± 0.05, N/H < 10^{-3} and O/H = 0.003 ± 0.002. Hence, this object has a high carbon abundance (C/He = 0.3) in common with many PG1159 stars but has a much higher hydrogen abundance (H/He = 2) than e.g. PG1159−035 (H/He < 0.2; Werner 1996). HS 2324+3944 also differs from the typical PG1159 star in that it has a relatively low oxygen abundance (O/He = 0.006). HS 2324+3944 lies on our $Z = 0.004$, $M = 0.9\,{\rm M}_{\odot}$, $M_{\rm WD} = 0.550\,{\rm M}_{\odot}$, AGB departure type II track in the $\log T_{\rm eff}$–$\log g$ diagram. At $\log g = 6.2$, the model abundances are He/H = 4, C/H = 0.5, N/H = 0.03 and O/H = 0.06, which indicates that the model is too depleted in H relative to HS 2324+3944. At $\log g = 5$, the model abundances are He/H = 0.5, C/H = 0.4, N/H = 10^{-3} and O/H = 0.005, which agrees well with the observed ratios except that carbon abundance is too high by a factor of about 2. This comparison again suggests that our adopted mass-loss rates are too high for the post-AGB phases of the evolution. Indeed, a reduction in mass-loss rate by a factor of 2 since the model star left the AGB would give the needed delay in the time at which the surface hydrogen abundance is reduced to the observed value. Such a reduction would have been obtained for the hot stages of evolution if we had used the mass-loss rates of Pauldrach et al. (1988).

8.2 White dwarf asteroseismology

From their asteroseismological analysis of the prototypical DBv, GD 358, Bradley & Winget (1994) determined a stellar mass $M_* = 0.61 \pm 0.03\,{\rm M}_{\odot}$, and a helium layer mass of $\log M_{\rm He}/M_* = -5.70^{+0.18}_{-0.30}$. This helium layer mass is much smaller than the 'canonical' value of $10^{-2}\,M_*$ from stellar evolution theory (e.g. Iben 1989; D'Antona & Mazitelli 1991) for a 0.6 $\rm M_{\odot}$ remnant. It is also three orders of magnitude smaller than the mass of helium found by asteroseismological analysis of PG1159 (Kawaler & Bradley 1994), a likely predecessor of cool DB white dwarfs. In order to investigate a possible evolutionary link between these two objects, Dehner & Kawaler (1995) computed evolutionary sequences of cooling white dwarfs that included time-dependent diffusion processes in a similar way to Iben & MacDonald (1985). Their starting model had an initial effective temperature of 140 000 K and a surface layer of mass $3 \times 10^{-3}\,M_*$ with uniform composition of 30 per cent helium, 35 per cent carbon and 35 per cent oxygen. Below this surface layer, the composition changed to 50 per cent carbon and 50 per cent oxygen. By the time the effective temperature has dropped to that of GD 358, the diffusion processes have modified the composition profile in such a way that there is a broad He/C transition zone centred near a mass depth of $10^{-6}\,M_*$. The pulsation spectrum of the model matches reasonably well the observed spectrum. However, a comparison with the He masses in Table 5 shows that $3 \times 10^{-3}\,M_*$ is an order of magnitude smaller than we find for a 0.6 $\rm M_{\odot}$ remnant, and hence an inconsistency remains between the asteroseismological and evolutionary mass determinations. Furthermore, MacDonald et al. (1998) have shown that scenarios in which GD 358 is a descendant of a PG1159-like star suffer from an inconsistency between the requirement that the helium layer mass be consistent with asteroseismology and the requirement that it be very small for C to be present in the photosphere at the observed abundance of log n(C)/n(He) = -5.65 ± 0.10 (Provencal et al. 1996). More recently Montgomery, Metcalfe & Winget (2003) have found a symmetry in the way that high-overtone stellar pulsations sample the structure of the core and the envelope which can lead to an ambiguity in the asteroseismological determination of the location of internal transitions. In the specific case of GD 358, they find that a transition from a C/O mixture to a nearly pure C composition near 0.5 M_* could be mimicked by an envelope transition zone at $10^{-6}\,M_*$. A sharp transition in C/O ratio at the required location is found in the evolutionary models of Salaris et al. (1997) and Metcalfe, Salaris & Winget (2002) but not in the models of Althaus et al. (2002). Fig. 13 shows carbon and oxygen mass fractions for the 0.597 $\rm M_{\odot}$ white dwarf remnant of our $Z = 0.02$ star of initial mass 2 $\rm M_{\odot}$. We see that there is a clear transition in C-to-O ratio over the mass range 0.5–0.55 M_*. This corresponds to the location of the edge of the CO core at the end of core helium burning. Hence, the possibility remains that the low He-layer masses derived from some asteroseismological studies are incorrect and that He-layer masses of $\sim 10^{-2}$ $\rm M_{\odot}$, in accord with stellar evolution calculations, are possible.

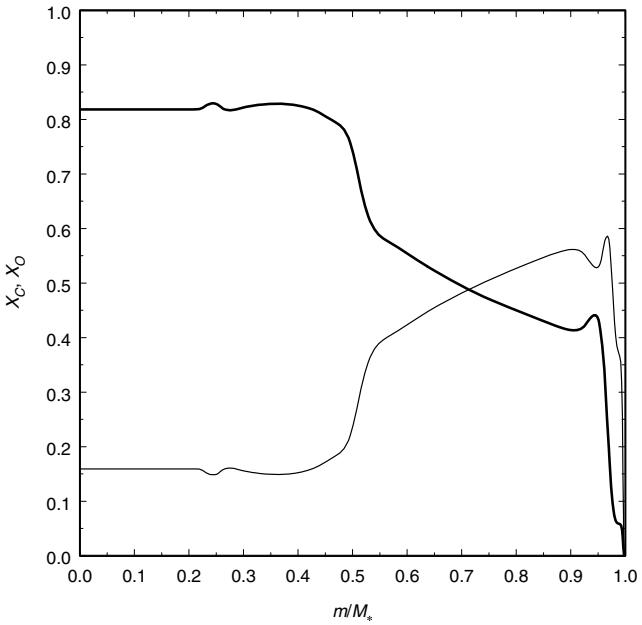

Figure 13. Mass fraction of oxygen (thick line) and carbon (thin line) against mass coordinate for the 0.597 $\rm M_{\odot}$ white dwarf remnant of a star of initial mass $M = 2\,{\rm M}_{\odot}$ and heavy element abundance $Z = 0.02$.

8.3 DQ white dwarfs

The widely accepted mechanism for formation of DQ white dwarfs, initially proposed by Koester et al. (1982), is that as the star cools the envelope convection zone grows inwards and dredges up carbon diffusing outwards from the interior. This idea was explored further by Pelletier et al. (1986) and MacDonald et al. (1998) with the latter paper also including oxygen in the simulations. This scenario has been modified by Fontaine & Brassard (2005), who find that the carbon pollution is not produced by carbon diffusing outward from the core but by the inward growth of superficial helium convection zone catching up some of the settling carbon and bringing it to the surface. These studies show that the final value of $\Delta M_{\rm buff}$ controls the amount of C and O that can be convectively dredged to the surface, with smaller helium masses leading to larger C and O abundances in the photosphere. In either scenarios, for white dwarfs of known mass, the observed surface abundances can, in principle, be used to estimate the helium mass. Recently, Dufour, Bergeron & Fontaine (2005) have re-analysed spectrometric and photometric observations of 16 cool DQ white dwarfs from the Bergeron, Ruiz & Leggett (1997) and Bergeron, Leggett & Ruiz (2001) sample to obtain effective temperatures, masses and carbon abundances. They find that the DQ stars have the mean mass of 0.62 $M_\odot$ and that n(C)/n(He) is strongly anticorrelated with effective temperature. Using the Fontaine & Brassard (2005) models for their single white dwarf mass of 0.6 $M_\odot$, Dufour et al. (2005) find that the n(C)/n(He) ratios for the majority of the DQs are consistent with a helium layer mass between 10^{-3} and $10^{-2}\,M_*$.

Because helium envelope white dwarfs are the descendants of stars that leave the AGB-burning helium or experience a VLTP, their helium masses are expected to be near the lower end of the possible range. For $M_{\rm WD} = 0.6$ $M_\odot$, we estimate that the relevant range for helium mass is 10^{-2}–$2 \times 10^{-2}\,M_*$, which is marginally consistent with the range found by Dufour et al. (2005). However, the amount of C enrichment is also strongly dependent on white dwarf mass (Pelletier et al. 1986; MacDonald et al. 1998). Further calculations of DQ evolution at different white dwarf masses are still needed before a meaningful comparison between helium masses from stellar evolution calculations and those from DQ C abundances can be carried out.

8.4 Self-induced novae

Iben & MacDonald (1986) found that the condition for a white dwarf to experience a final hydrogen shell flash due to inward diffusion of hydrogen and outward diffusion of carbon into regions hot enough for nuclear reactions to occur is

$$M_{\rm buf} < M_{\rm buf}^{\rm crit} \approx 0.1 \Delta M_{\rm H}. \qquad (12)$$

By comparing the values for $\overleftrightarrow{M}_{\rm buf,min}$ and $\Delta M_{\rm H}$ in Table 7, we see that $\overleftrightarrow{M}_{\rm buf,min} \gtrsim 0.4 \Delta M_{\rm H}$ and hence we conclude that conditions for the self-induced nova do not occur for progenitor masses less than 3 $M_\odot$.

9 CONCLUSIONS

We have shown, for evolution of single stars that do not experience a VLTP, that the mass of helium remaining on a white dwarf star lies between limits that depend primarily on the mass of the white dwarf and only weakly on the heavy element abundance in the progenitor. Also we find that stars that experience a VLTP have final helium masses that are about 25 per cent below the lower limit.

Following Iben (1987), we have derived a criterion, based on the phase of the thermal pulse cycle at which the star leaves the AGB, for determining if a star will experience a post-AGB helium shell flash and subcriteria for discriminating between the occurrence of late and VLTPs. We find that a post-AGB flash does not necessarily result in formation of a non-DA white dwarf. Furthermore, we find that the relative amount of time spent burning helium or hydrogen depends on how the mass-loss rate varies with stellar surface parameters. These two considerations complicate the relationship between the probability that a star experiences a post-AGB flash and the relative formation rates of DA and non-DA white dwarfs. Although small in number, our calculations do lead to a non-DA/DA ratio that is consistent with the observed ratio, which suggests that our adopted mass-loss rates are reasonable. This conclusion is supported by our initial mass–final mass relation being consistent with observation.

We find that our predicted abundances for PG1159 stars agree within the error bars with the observed abundances, without the need of convective overshoot. We also find that nitrogen is produced during VLTPs but not in the other evolutionary paths to hydrogen-deficient objects. Hence, we propose this as the reason why nitrogen is observed in some PG1159 stars but not all. Our VLTP models also produce surface abundances close to those of the low-gravity hybrid PG1159 stars.

ACKNOWLEDGMENTS

We are grateful to Stefan Dreizler, Judi Provencal and Richard Townsend for helpful correspondence and discussions. We also thank the referee for constructive comments. This work has been supported in part by the Annie Jump Cannon fund at the University of Delaware and by funds from Penn State University at Wilkes-Barre.

REFERENCES

Abbott D., 1982, ApJ, 259, 282
Alexander D. R., Ferguson J. W., 1994, ApJ, 437, 879
Althaus L. G., Serenelli A. M., Córsico A. H., Benvenuto O. G., 2002, MNRAS, 330, 685
Angulo C. et al., 1999, Nucl. Phys. A, 656, 3
Arnett D., 1996, Supernovae and Nucleosynthesis: An Investigation of the History of Matter, from the Big Bang to the Present. Princeton Univ. Press, Princeton, NJ
Beaudet G., Petrosian V., Salpeter E. E., 1967, ApJ, 150, 979
Bergeron P., Ruiz M. T., Leggett S. K., 1997, ApJS, 108, 339
Bergeron P., Leggett S. K., Ruiz M. T., 2001, ApJS, 133, 413
Blöcker T., 2001, Ap&SS, 275, 1
Blöcker T., Schönberner D., 1997, A&A, 324, 991
Boothroyd A. I., Sackmann I.-J., 1988, ApJ, 328, 671
Bradley P. A., Winget D. E., 1994, ApJ, 430, 850
Brocato E., Castellani V., Ripepi V., 1995, AJ, 109, 1670
Buonanno R., Corsi C. E., Fusi Pecci F., 1981, MNRAS, 196, 435
Caputo F., Chieffi A., Tornambe A., Castellani V., Pulone L., 1989, ApJ, 340, 241
Castellani V., Giannone P., Renzini A., 1971, Ap&SS, 10, 340
Castellani V., Chieffi A., Pulone L., Tornambe A., 1985, ApJ, 296, 204
Caughlan G. R., Fowler W. A., 1988, At. Data Nucl. Data Tables, 40, 283
D'Antona F., Mazitelli I., 1991, in Michaud G., Tutukov A. V., eds, Proc. IAU Symp. 145, Evolution of Stars: The Photospheric Abundance Connection. Kluwer, Dordrecht, p. 399
Dehner B. T., Kawaler S. D., 1995, ApJ, 445, L141
Dreizler S., Heber U., 1998, A&A, 334, 618
Dreizler S., Werner K., 1996, A&A, 314, 217
Dreizler S., Werner K., Heber U., Engels D., 1996, A&A, 309, 820

Dufour P., Bergeron P., Fontaine G., 2005, ApJ, 627, 404
Edvardsson B., Andersen J., Gustafsson B., Lambert D. L., Nissen P. E., Tomkin J., 1993, A&A, 275, 101
Eggleton P. P., 1971, MNRAS, 151, 351
Eggleton P. P., 1972, MNRAS, 156, 361
Eggleton P. P., Faulkner J., Flannery B. P., 1973, A&A, 23, 325
Feast M. W., Glass I. S., Whitelock P. A., Catchpole R. M., 1989, MNRAS, 241, 375
Fontaine G., Brassard P., 2002, ApJ, 581, L33
Fontaine G., Brassard P., 2005, in Koester D., Moehler S., eds, ASP Conf. Ser. Vol. 334, Proc. 14th European Workshop on White Dwarfs. Astron. Soc. Pac., San Francisco, p. 49
Fontaine G., Graboske H. C. Jr, van Horn H. M., 1977, ApJS, 35, 293
Fowler W. A., Caughlan G. R., Zimmerman B. A., 1975, ARA&A, 13, 69
Frost C. A., Lattanzio J. C., 1996, ApJ, 473, 383
Fujimoto M. Y., 1977, PASJ, 29, 331
Girardi L., Bressan A., Bertelli G., Chiosi C., 2000, A&AS, 141, 371
Greenstein J. L., 1986, ApJ, 304, 334
Groenewegen M. A. T., Whitelock P. A., 1996, MNRAS, 281, 1347
Haft M., Raffelt G., Weiss A., 1994, ApJ, 425, 222
Harris M. J., Fowler W. A., Caughlan G. R., Zimmerman B. A., 1983, ARA&A, 21, 165
Herald J. E., Bianchi L., 2004, ApJ, 611, 294
Herwig F., 2001, ApJ, 554, L71
Herwig F., Blöcker T., Schönberner D., El Eid M., 1997, A&A, 324, L81
Herwig F., Blöcker T., Langer N., Driebe T., 1999, A&A, 349, L5
Heske A., Forveille T., Omont A., van der Veen W. E. C. J., Habing H. J., 1990, A&A, 239, 173
Hillier D. J., 2003, in van der Hucht K. A., Herrero A., Esteban C., eds, Proc. IAU Symp. 212, A Massive Star Odyssey: From Main Sequence to Supernova. Astron. Soc. Pac., San Francisco, p. 70
Hügelmeyer S. D., Dreizler S., Werner K., Nitta A., Kleinman S. J., Krzesinski J., 2005, in Koester D., Moehler S., eds, ASP Conf. Ser. Vol. 334, Proc. 14th European Workshop on White Dwarfs. Astron. Soc. Pac., San Francisco, p. 233
Iben I., 1975, ApJ, 196, 525
Iben I., 1984, ApJ, 277, 333
Iben I., 1987, Late Stages of Stellar Evolution, Reidel, Dordrecht, p. 175
Iben I., 1989, in Johnson H. R., Zuckerman B., eds, Proc. IAU Coll. 106, Evolution of Peculiar Red Giant Stars. Cambridge Univ. Press, Cambridge, p. 205
Iben I., MacDonald J., 1985, ApJ, 296, 540
Iben I., MacDonald J., 1986, ApJ, 301, 164
Iben I., MacDonald J., 1995, in Koester D., Werner K., eds, Lecture Notes in Physics, Vol. 443, Proc. 9th European Workshop on White Dwarfs. Springer-Verlag, Berlin, p. 48
Iben I., Kaler J. B., Truran J. W., Renzini A., 1983, ApJ, 264, 605
Iben I., Fujimoto M. Y., MacDonald J., 1992, ApJ, 388, 521
Iben I., Tutukov A. V., Yungelson L. R., 1996, ApJ, 456, 750
Iglesias C. A., Rogers F. J., 1996, ApJ, 464, 943
Itoh N., Kohyama Y., 1983, ApJ, 275, 858
Itoh N., Totsuji H., Ichimaru S., Dewitt H. E., 1979, ApJ, 234, 1079
Jimenez R., MacDonald J., 1996, MNRAS, 283, 721
Jimenez R., Thejll P., Jørgensen U. G., MacDonald J., Pagel B., 1996, MNRAS, 282, 926
Jimenez R., Flynn C., MacDonald J., Gibson B. K., 2003, Sci, 299, 1552
Jimenez R., MacDonald J., Dunlop J. S., Padoan P., Peacock J. A., 2004, MNRAS, 349, 240
Karakas A. I., Lattanzio J. C., Pols O. R., 2002, Publ. Astron. Soc. Aust. 19, 515
Kawaler S. D., Bradley P. A., 1994, ApJ, 427, 415
Knapp G. R., Young K., Lee E., Jorissen A., 1998, ApJS, 117, 209
Koesterke L., Werner K., 1998, ApJ, 500, L55
Koester D., Weidemann V., Zeidler E.-M., 1982, A&A, 116, 147
Kogut A. et al., 2003, ApJS, 148, 161
Kudritzki R.-P., Puls J., 2000, ARA&A, 38, 613
Kudritzki R.-P., Pauldrach A., Puls J., 1987, A&A, 173, 293
Lattanzio J., Frost C., Cannon R., Wood P. R., 1996, Mem. Soc. Astron. Ital., 67, 729
Lawlor T. M., MacDonald J., 2003, ApJ, 583, 913 (LM03)
Lejeune T., Schaerer D., 2001, A&A, 366, 538
Lepine J. R. D., Ortiz R., Epchtein N., 1995, A&A, 299, 453
Leuenhagen U., Hamann W.-R., Jeffery C. S., 1996, A&A, 312, 167
MacDonald J., Hernanz M., Jose J., 1998, MNRAS, 296, 523
Mansoori G. A., Carnahan N. F., Starling K. F., Leland T. W., 1971, J. Chem. Phys., 54, 1523
Marigo P., Girardi L., Bressan A., 1999, A&A, 344, 123
Metcalfe T. S., Salaris M., Winget D. E., 2002, ApJ, 573, 803
Metcalfe T. S., Montgomery M. H., Kawaler S. D., 2003, MNRAS, 344, 88
Michaud G., 1987, in Phillip A. G. D., Hayes D. S., Liebert J., eds, Proc. IAU Coll. 95, The Second Conference on Faint Blue Stars. Davis Press, Schenectady, NY, p. 249
Mihalas D., 1970, Stellar Atmospheres. Freeman & Co., San Francisco
Montgomery M. H., Metcalfe T. S., Winget D. E., 2003, MNRAS, 344, 657
Mowlavi N., 1999, A&A, 344, 617
Mowlavi N., Schaerer D., Meynet G., Bernasconi P. A., Charbonnel C., Maeder A., 1998, A&AS, 128, 471
Napiwotzki R., 1999, A&A, 350, 101
Napiwotzki R., Schönberner D., 1991, A&A, 249, L16
Nomoto K., Thielemann F.-K., Miyaji S., 1985, A&A, 149, 239
Ostlie D. A., Cox A. N., 1986, ApJ, 311, 864
Paczynski B., 1974, ApJ, 192, 483
Pauldrach A., Puls J., Kudritzki R. P., Mendez R. H., Heap S. R., 1988, A&A, 207, 123
Peimbert A., Peimbert M., Luridiana V., 2002, ApJ, 565, 668
Pelletier C., Fontaine G., Wesemael F., Michaud G., Wegner G., 1986, ApJ, 307, 242
Pols O. R., Tout C. A., 2001, Mem. Soc. Astron. Ital., 72, 299
Provencal J. L., Shipman H. L., Thejll P., Vennes S., Bradley P. A., 1996, ApJ, 466, 1011
Ramadurai S., 1976, MNRAS, 176, 9
Reddy B. E., Tomkin J., Lambert D. L., Allende Prieto C., 2003, MNRAS, 340, 304
Reimers D., 1975, Mem. R. Soc. Sci. Liege, 8, 369
Renzini A., 1979, in Westerlund B. E., ed., Proc. Fourth European Regional Meeting in Astronomy, ASSL Vol. 75, Stars and Star Systems. Reidel, Dordrecht, p. 155
Renzini A., 1981, in Chiosi C., Stalio R., eds, Proc. IAU Coll. 59, ASSL Vol. 89, Effects of Mass Loss on Stellar Evolution. Reidel, Dordrecht, p. 319
Renzini A., 1983, in Flower D. R., ed., Proc. IAU Symp. 103, Planetary Nebulae. Reidel, Dordrecht, p. 267
Ritossa C., García-Berro E., Iben I., 1996, ApJ, 460, 489
Salaris M., Dominguez I., García-Berro E., Hernanz M., Isern J., Mochkovitch R., 1997, ApJ, 486, 413
Salpeter E. E., van Horn H. M., 1969, ApJ, 155, 183
Schaller G., Schaerer D., Meynet G., Maeder A., 1992, A&AS, 96, 269
Schild H. et al., 2004, A&A, 422, 177
Schönberner D., 1979, A&A, 79, 108
Sion E. M., 1984, ApJ, 282, 612
Spergel D. N. et al., 2003, ApJS, 148, 175
Stancliffe R. J., Izzard R. G., Tout C. A., 2005, MNRAS, 356, L1
Stringfellow G. S., DeWitt H. E., Slattery W. L., 1990, Phys. Rev. A, 41, 1105
Sugimoto D., 1970, ApJ, 159, 619
Unglaub K., Bues I., 1998, A&A, 338, 75
Vassiliadis E., Wood P. R., 1993, ApJ, 413, 641
Vassiliadis E., Wood P. R., 1994, ApJS, 92, 125
Vink J. S., de Koter A., Lamers H. J. G. L. M., 2001, A&A, 369, 574
Weidemann V., 2000, A&A, 363, 647
Werner K., 1996, A&A, 309, 861
Werner K., Herwig F., 2006, PASP, 118, 183
Werner K., Dreizler S., Heber U., Kappelmann N., Kruk J., Rauch T., Wolff B., 1997, Rev. Mod. Astron., 10, 219

Werner K., Rauch T., Reiff E., Kruk J. W., Napiwotzki R., 2004, A&A, 427, 685
Whitelock P., Menzies J., Feast M., Marang F., Carter B., Roberts G., Catchpole R., Chapman J., 1994, MNRAS, 267, 711
Whitelock P. A., Feast M. W., van Loon J. Th., Zijlstra A. A., 2003, MNRAS, 342, 86
Willson L. A., 2000, ARA&A, 38, 573
Winkler K.-H. A., Norman M. L., Newman M. J., 1984, Physica D, 12, 408
Wood P. R., Faulkner D. J., 1986, ApJ, 307, 659

This paper has been typeset from a TEX/LATEX file prepared by the author.